LT-XFD_CDR_XPD-00119

NSLS-II Project

CONCEPTUAL DESIGN REPORT for the

X-RAY POWDER DIFFRACTION BEAMLINE AT NSLS-II

final draft Sep 2009

Intentionally blank.

Approvals and Reviewers

Compiled by	**Signature**	**Date**
Eric Dooryhee, Beamline Scientist, NSLS-II		
Reviewers		
Simon Billinge, BAT Spokesperson, signing on behalf of the BAT		
Andy Broadbent, Beamlines Manager		
Nicholas Gmür, ESH Coordinator, NSLS-II		
Sushil Sharma, Mechanical Engineering Group Leader, NSLS-II		
Approvals		
Qun Shen, XFD Director, NSLS-II		

Document Updates

The Conceptual Design Report for the Beamlines Infrastructure at NSLS-II is a controlled document, revised under change control.

Version No.	Date	Authorized by	Changes made
A	9/30/2009	E. Dooryhee	Final release
1	10/1/2009		final draft, submitted to BAT

Intentionally blank.

Contents

1. INTRODUCTION 1
   - 1.1 Scientific Issues 1
   - 2.2 Beamline Advisory Team (BAT) 1
   - 1.3 Representative Experiments 2
   - 1.4 Acknowledgments 2
2. BEAMLINE LAYOUT 3
   - 2.1 Overview 3
   - 2.2 Insertion Device 6
   - 2.3 Front End 9
   - 2.4 Optical Layout 11
     - 2.4.1 Main Branch 16
     - 2.4.2 Side-Branch 16
     - 2.4.3 Sector Layout 16
   - 2.5 High Heatload Optics 16
   - 2.6 Major Components 18
     - 2.6.1 Horizontal Deflecting Side Bounce Monochromator 19
     - 2.6.2 Sagittally-Focusing Double-Crystal Laue Monochromator 20
     - 2.6.3 Focusing optics 22
   - 2.7 Summary of Beamline Performance Specifications 24
3. END STATION INSTRUMENTATION 25
   - 3.1 High Energy X-ray Detectors 26
   - 3.2 High-Resolution Analyzer Stage 26
   - 3.3 Software Development 27
   - 3.4 Complementary Experimental Stations 27
   - 3.5 Sample Environment 28
4. SPECIAL BEAMLINE REQUIREMENTS 29
5. FUTURE UPGRADE OPTIONS 30
6. SUMMARY 31
7. REFERENCES 32

APPENDIX 1 SCHEDULE 33
APPENDIX 2 REFERENCE DRAWINGS 34
APPENDIX 3 REPRESENTATIVE EXPERIMENTS 38
APPENDIX 4 THERMAL CALCULATIONS 40
APPENDIX 5 LAUE MONOCHROMATIZATION 42
- Horizontal Deflecting Side Bounce Monochromator 42
- Sagittally-Focusing Double-Crystal Laue Monochromator 43

APPENDIX 6 REFRACTIVE OPTICS 46
APPENDIX 7 DETECTOR DEVELOPMENT 47

Acronyms

Be	beryllium
CDR	Conceptual Design Report
CO	Lead Collimator
CRL	Compound Refractive Lens
DLCM	Double Laue Crystal Monochromator
ES	End Station
EXAFS	Extended X-ray Absorption Fine Structure
FAPM	Fixed Aperture Mask
FE	Front End
FEA	Finite Element Analysis
FGV	Fast Gate Valve
FOE	First Optics Enclosure
FZP	Fresnel Zone Plates
HOPG	Highly Oriented Pyrolytic Graphite
NMR	Nuclear Magnetic Resonance
PDF	Pair Distribution Function
SBM	Side Bounce Monochromator
SGV	Slow Gate Valve
SS	Safety Shutter
XBPM	Photon Beam Position Monitor

1. INTRODUCTION

1.1 Scientific Issues

The primary purpose of this beamline is the quantitative characterization of the atomic structure of complex materials; not just carefully-prepared ideal systems, but materials as they are actually used. Detailed knowledge of atomic structure is a prerequisite to understanding material properties, and essential in any rational materials design and synthesis effort. Development of meaningful structure/property correlations requires simultaneous measurement of structure and properties.

The scientific grand challenge is to obtain robust and quantitative (micro)structural information about materials that are complex, nanostructured and often heterogeneous. As well as studying structure in the ground state at ambient conditions, it is increasingly important to study structure in systems that are evolving in time (for example, after excitation or while undergoing chemical reaction), and materials that are in a metastable state. These situations are becoming the norm rather than the exception in frontier science and technology, but we are far from having robust tools for studying structure in such systems. Finally, an important scientific goal is the study of materials under extreme conditions of temperature, pressure, magnetic/electric/stress field, chemical environment, etc. Such study presents special challenges to the experimentalist, not only in generating the extreme conditions, but in getting the x-ray probe into and out of the apparatus.

The proposed X-ray Powder Diffraction (XPD) beamline will provide unique capabilities for addressing these problems, and is designed with Total Structure Studies in mind. High-throughput, high-resolution powder diffraction (with well-defined peak shapes and extremely low background) will be carried out using hard x-rays, with a beam size (tens to hundreds of microns) adjustable to match the graininess and heterogeneity scales. The need for high resolution applies either in reciprocal space or in direct space or more rarely in both. The combination with a complementary parallel operation side-station for high-throughput, high-Q, Pair Distribution Function studies (also with small beams) will permit determination of both long- and short-range structures. Moreover the beamline will pay special attention to sample environments, allowing for time-resolved and in situ measurements.

The XPD beamline will build upon active programs at the NSLS (and elsewhere), concentrating on higher energies (40-100 keV). In conventional x-ray diffraction, any energy greater than 20keV is considered exotically high. The beamline must address future scientific challenges in (for example) hydrogen storage, CO2 sequestration, advanced structural ceramics, catalysis, and materials processing—all in situ/in operando experiments difficult at other national user facilities. The beamline will also be of novel optical design, making use of techniques and instrumentation pioneered at the NSLS (Laue monochromators and Ge strip array detectors), as well as being perfectly matched to the high flux of a full 7m NSLS-II damping wiggler.

2.2 Beamline Advisory Team (BAT)

The XPD Beamline Advisory Team (BAT), formed in March 2008, is a group of expert scientists with common interest and experience in the XPD scientific program and the beamline optics and endstations needed to carry out this forefront program. The members are as follows:

Simon Billinge (spokesperson)	Columbia University and BNL
Peter Chupas	Argonne National Laboratory
Lars Ehm	Stony Brook University
Jon Hanson	Brookhaven National Laboratory
James Kaduk	Poly Crystallography Inc.
John Parise	Stony Brook University
Peter Stephens	Stony Brook University

Sign-up agreement between NSLS-II Project Director Steve Dierker and the Beamline Advisory Team, 11/24/2008.

1.3 Representative Experiments

The source for the beamline will be a full length 7m long damping wiggler to obtain the highest possible flux in the desired energy range of 40-100keV, with optimization at ~50keV and ~80keV. The advantages of hard x-rays are the ability to penetrate thick samples and environmental chambers, to provide access to a larger portion of reciprocal space, and to access reciprocal diffraction vectors Q as large as 60Å^{-1}. The scattering geometry is also simplified because of the large Ewald sphere and allows for transmission diffraction. Most importantly, absorption corrections are minimal and yield more accurate diffracted intensities.

Recent examples of high-energy x-ray research include measurements of stress/strain in materials, powder diffraction of compounds containing heavy elements, diffuse scattering of defects in complex oxides, high/small-angle scattering from thermal-barrier coatings, imaging and tomography. In short, the major proposed XPD beamline scientific program areas are:

- Complexity and the nanostructure problem
- Extreme environments
- Time resolved studies
- Total structure studies

In particular, next-generation technologies will place increasing demands on materials, requiring enhanced functionality and performance under extreme environments. The ability to design functional materials at the atomic level, taking advantage of new synthetic approaches and computational modeling, unavoidably requires dedicated characterization tools with an increasing level of sophistication and hardware/software integration. Specific examples are given in Appendix 3.

1.4 Acknowledgments

All BNL staff below are acknowledged for help, support, and discussion and for providing relevant material (calculations, figures, drawings, etc.). ACCEL (now Bruker) is also thanked for providing the preliminary case study and design for the XPD project beamline.

Qun Shen, Director, Experimental Facilities Division (XFD), NSLS-II, BNL

Lonny Berman, Head of the Beamline R&D Section, Experimental Systems Division (ESD), NSLS, BNL

Andy Broadbent, Beamlines Manager, XFD, NSLS-II, BNL

Mary Carlucci-Dayton, Mechanical Engineer, XFD, NSLS-II, BNL

Oleg Chubar, Beamline Scientific Support, XFD, NSLS-II, BNL

Lewis Doom, Mechanical Engineering Division, NSLS-II, BNL

Kenneth Evans-Lutterodt, physicist, ESD, NSLS, BNL

Konstantine Kaznatcheev, Beamline Scientific Support, XFD, NSLS-II, BNL

Paul Northrup, physicist, Environmental Sciences Department, BNL

Viswanath Ravindranath, Mechanical Engineering Division, NSLS-II, BNL

Kathleen Robinson, Editor, NSLS-II, BNL

Xianbo Shi, intern, NSLS-II, BNL

Peter Siddons, Head of the Detectors Section, ESD, NSLS, BNL

Zhong Zhong, physicist, ESD, NSLS, BNL

Much of the required design and engineering work is performed in a "centralized" fashion, involving the whole suite of six project beamlines and the anticipated 50+ beamlines. This routinely involves tight collaborations between the scientific and engineering staff across the Experimental Facilities Division and the entire NSLS-II project. The design of the baseline front ends was performed, for instance, by the Mechanical Engineering Group in the Accelerator Systems Division. The beamline also uses resources from the same group for tasks such as FEA simulations, synchrotron and bremsstrahlung ray tracing, etc.

2. BEAMLINE LAYOUT

2.1 Overview

The technical design issues are:

- Energy range 50-90keV
- Energy resolution (mode 1: $\Delta E/E \sim 2 \times 10^{-4}$; mode 2: $\Delta E/E \sim 1 \times 10^{-3}$)
- Intensity ($>10^{13}$ photons/sec/0.1%BW)
- Flexibility of focal lengths and sizes (2mm-500μm, down to 10μm)
- Beam stability (intensity and position)
- Low background and high filtering of forward, parasitic scattering and of low energy photons
- Employ proven technology whenever possible
- Ease of use
- Independent operation (shuttering) for the different hutches

The x-ray optics and beamline layout, shown in Figs. 1 and 2, are designed to operate two independent branch lines simultaneously. The angle deviation between the two beam axes is ~7.5 degrees, depending on the setting of the first monochromator. The first (upstream) endstation (ES1) covers most powder diffraction measurements, while the second endstation (ES2) is specialized in more elaborate/complex setups (large pressure cells, non routine reaction chambers, combined spectrometry, gas handling, user-defined specific devices). The downstream side station (ES3) will operate at a fixed high energy with very limited adjustability, and focuses on total scattering measurements over a large Q range. One main beamline target is the study of real samples in real time and in real conditions. By using a modular design for the endstations, special environments can be designed and inserted at different locations into the beamline with compatible interfaces. It is important all stations share the expertise, equipment, and software, and be operated more as a single entity. This is the reason why the floor occupation plan of the beamline allows us to easily move equipments and samples back and forth, in particular between ES1 ("standard" powder diffraction) and ES3 (PDF). The considerable divergence of the wiggler source, its high power output, and the low reflection angles in the x-ray high energy range are carefully handled in the present proposal: all three features put additional constraints on the optics and overall performance.

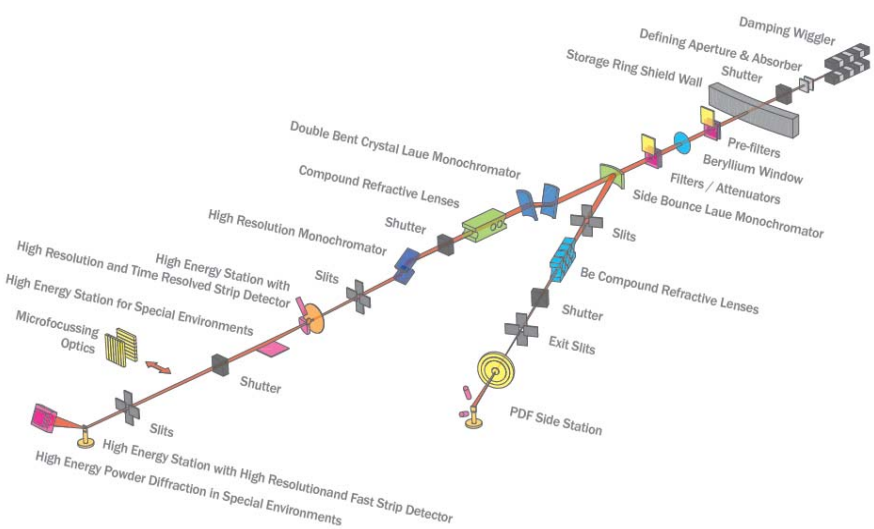

Fig. 1. Schematic layout of the beamline.

The horizontal radiation fan is more than 2mrad wide (FWHM). Focusing of the x-rays is thus crucial to collect the large fan in order to increase the available flux at the sample. Recent developments in sagittal focusing Laue optics make it possible to focus a large divergence of high-energy x-rays. The DOE review committee in June 2009 strongly recommended to "*include secondary optics into the design of the XPD beamline to provide 1-2micrometer focus.*" The DOE committee underlines: "Adding such optics should not have a significant impact on the beamline design while greatly broadening the user base for experiments that can be performed at the beamline. One example is the use of high-pressure cells." We are therefore carefully considering the ability to tune the beam size at will, in particular to resolve some particular inhomogeneities or for diffraction mapping. We propose here to achieve this goal by combining the sagittally bent double-Laue monochromator with CRL-based optics. A set of accurate hard x-ray slits and secondary focusing optics in hutch ES2 should allow a 10μm focus; this would be exceptional at these energies, and particularly suited for layered structures and heterogeneous compounds. The present design is provisioned for optimizing the beam size and beam intensity with 4 distinct focal lengths: at the sample or at the 2D detector either in hutch ES1, or in hutch ES2.

Fig. 2. Conceptual layout for the powder diffraction beamline. Top image, view from above. Scale 1/50.

2.2 Insertion Device

The powder diffraction beamline will be located at the damping wiggler source DW90 (12.5mm fixed gap), in a high-β straight-section of the NSLS-II ring. Unlike the NSLS-II undulator, bending-magnet and 3-pole wiggler sources, the NSLS-II damping wiggler extends the range of x-ray energies well beyond 50keV, thus allowing the study of samples under real conditions, i.e. in environmental chambers. This requires a dedicated strategy for handling the exceptional power output as well as significant shielding and thick enclosure walls. The power output of 65kW is unprecedented for a permanent magnet wiggler (the APS sector 11 wiggler produces 8kW for K=14, SPring-8 BL08W wiggler produces 14kW for K=10). The power density is about half that of the 14mm period superconducting undulator at its highest K. Power reduction (filtering) and high heat load optics merit careful investigation (see section 2.5).
The basic parameters for the damping wiggler source used in this design are shown in Tables 1 and 2.

Table 1. NSLS-II Machine and Damping Wiggler Parameters.

Electron energy, Eo	3 GeV
Electron current, Io	500 mA
Number of periods	70
Period length, λu	9 cm
Magnetic field	1.85 Tesla
Deflection parameter, k	15.8
Critical energy	10.8 keV

Table 2. RMS Electron Beam Values at the Center of the High-β Straight Section (9.3m).

Horizontal electron beam size, σ_x	137 μm
Vertical electron beam size, σ_z	4.9 μm
Horizontal electron beam divergence, σ_x'	6.6 μrad
Vertical electron beam divergence, σ_z'	1.6 μrad

Figs. 3 and 4 show the flux per unit horizontal angle and brightness values for the various NSLS-II sources. Fig. 4 shows the flux and brightness and compares the NSLS-II damping wiggler source and the existing NSLS X17 super-conducting wiggler (at the high-pressure diffraction beamline). The NSLS-II damping wiggler source exceeds the X17 source output and thus makes the proposed high-energy high-resolution powder diffraction beamline at the NSLS-II machine a very powerful facility.

Table 3. Brightness and flux of the Damping Wiggler source at NSLS II.

keV	Brightness (ph/sec/0.1%BW/mrad^2/mm^2)	Flux (ph/sec/0.1% BW/mrad)
40	6.8×10^{17}	4.5×10^{14}
60	1.7×10^{17}	8.8×10^{13}
80	3.8×10^{16}	1.7×10^{13}
100	7.9×10^{15}	3.1×10^{12}

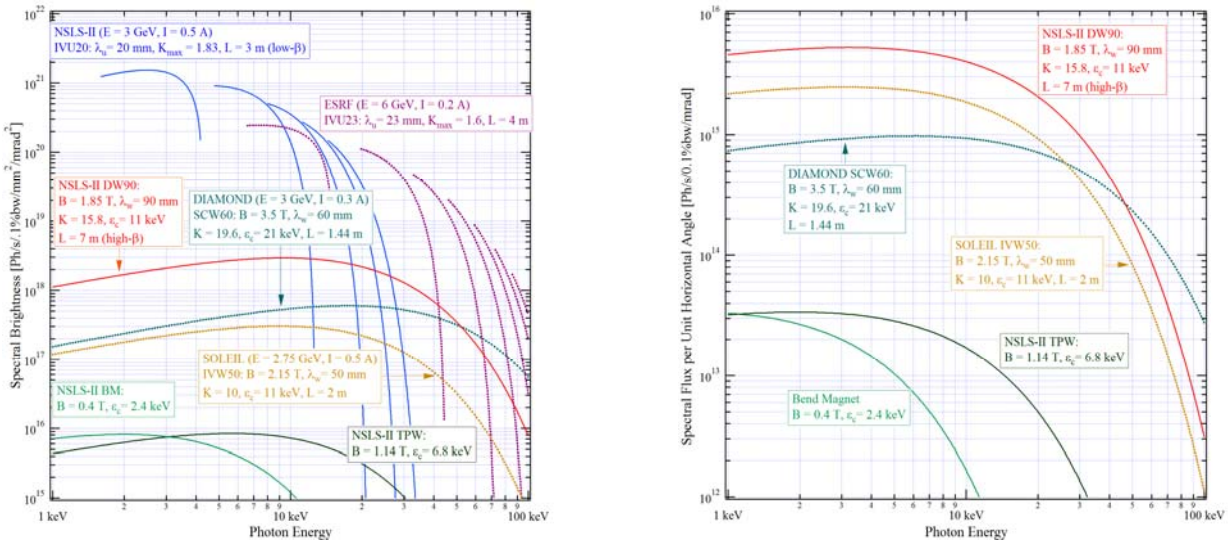

Fig. 3. Comparison of spectral brightness and spectral flux per unit of horizontal angle. (O. Tchoubar, NSLS-II)

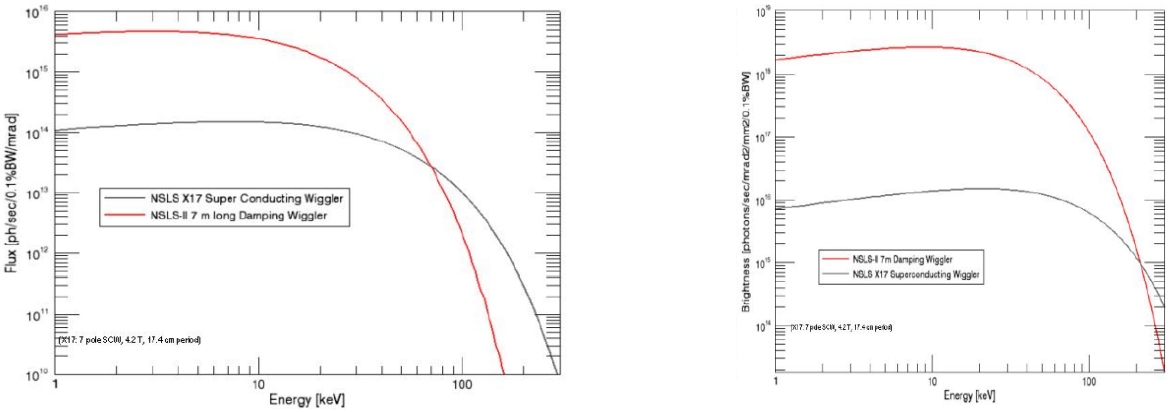

Fig. 4. Flux and brightness comparisons between the NSLS-II 7m-long DW source and the NSLS super-conducting wiggler.

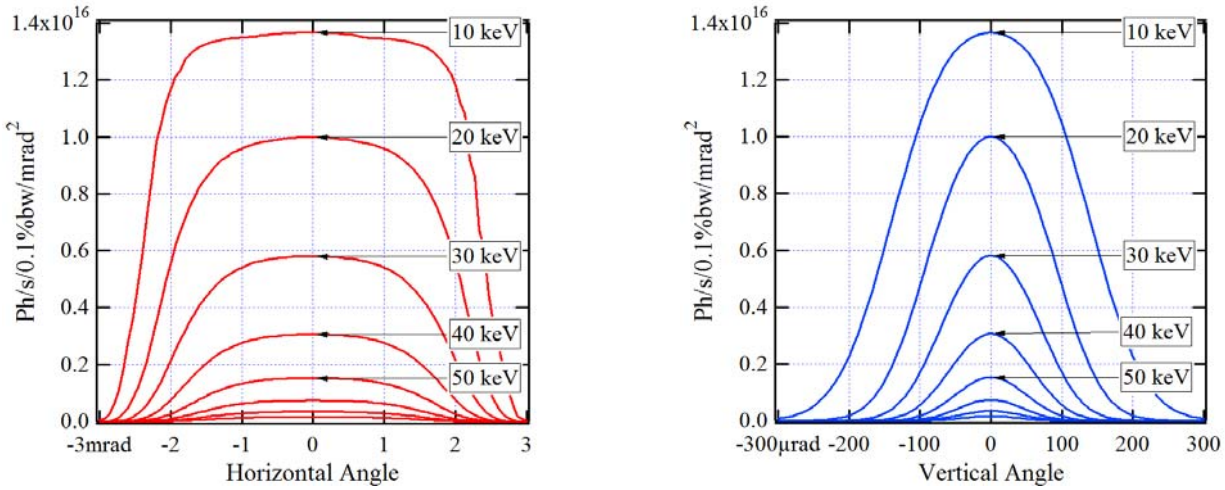

Fig. 5: Horizontal (left) and vertical (right) angular Profiles of DW Emission at Different Photon Energies. (O. Tchoubar, NSLS-II)

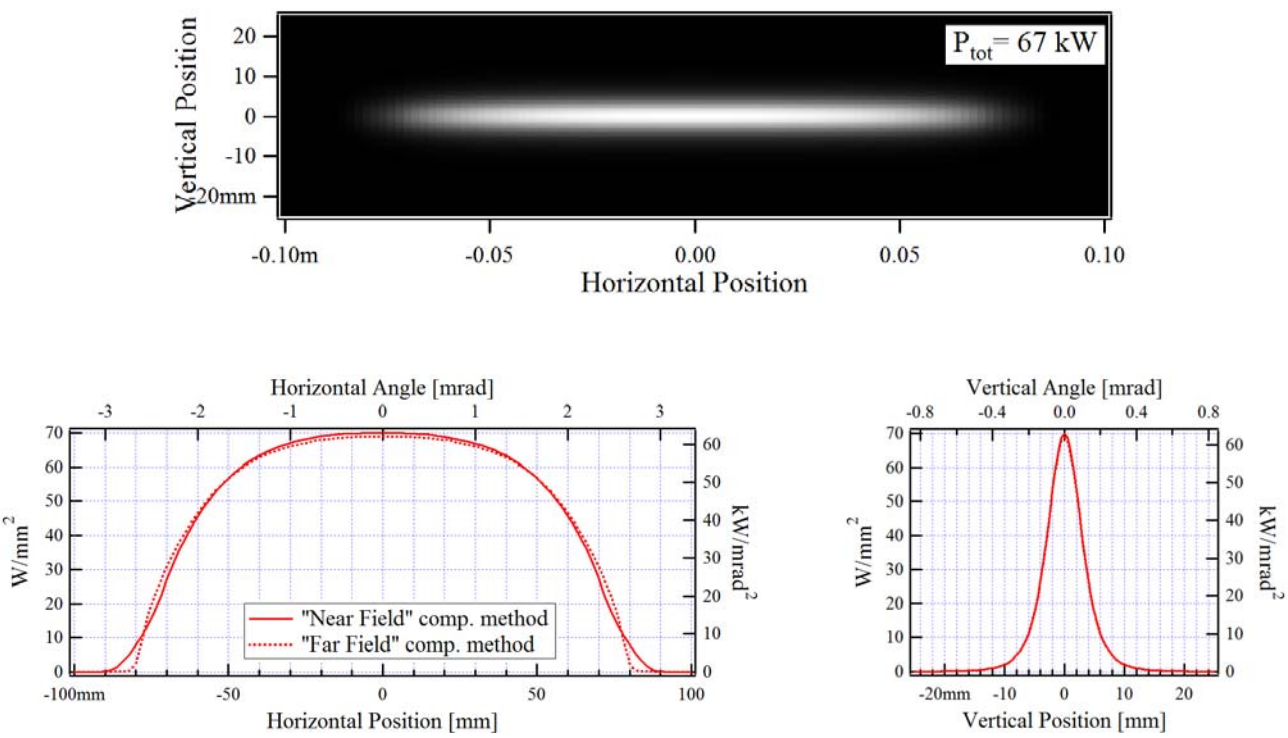

Fig. 6. Power Density Distribution in Transverse Plane at 30 m from Center of Straight Section. (O. Tchoubar, NSLS-II)

2.3 Front End

A layout of the standard NSLS-II front-end is shown in Fig. 7 and in appendix 2, and comprises: slow gate valve (SGV); fixed aperture mask (FM); photon beam position monitor; lead collimators (LCO and RCO); fast gate valve (FGV); safety shutters (SS, BMPS and PS); X,Y slits (XYSLT). The layout is shown in Appendix 2.

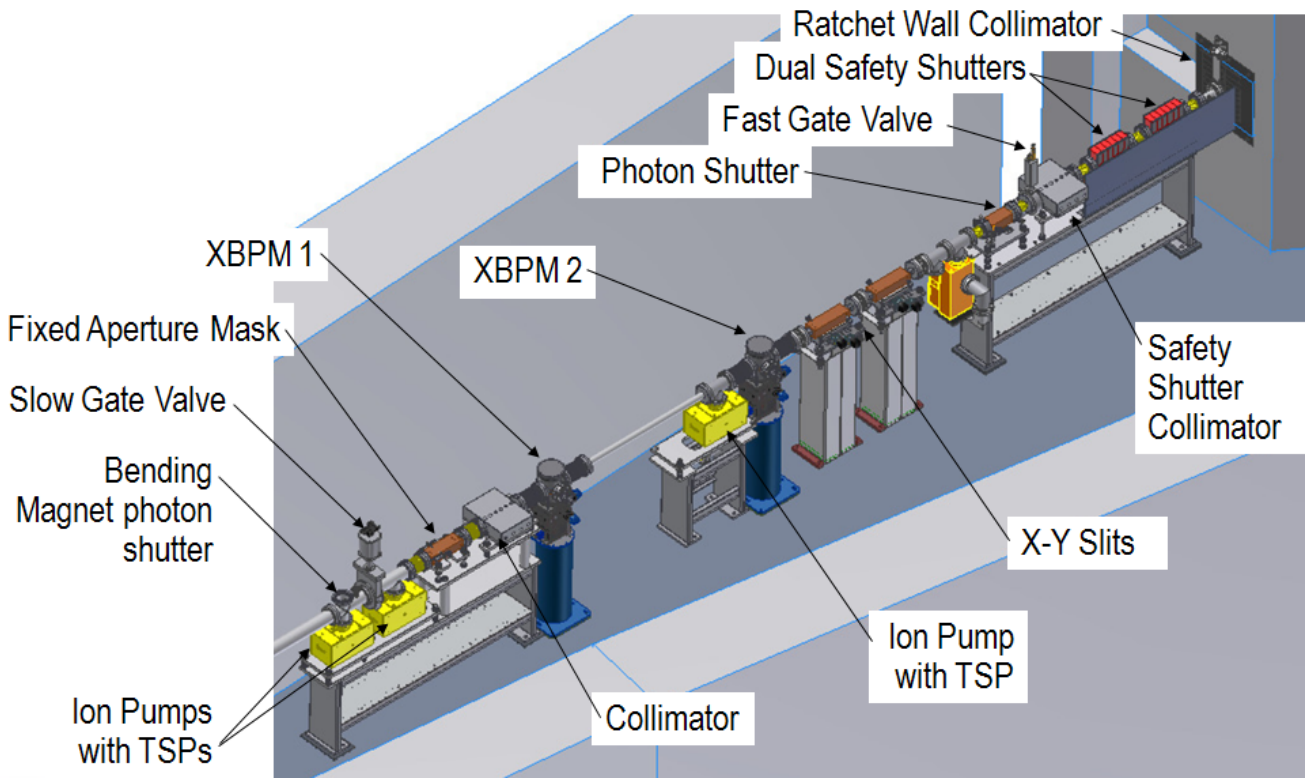

Fig. 7. Typical Front End Configuration at NSLSL II.

The basic configuration of the Damping Wiggler Front End is similar to the In-Vacuum Undulator front ends but must be able to accept the higher heat load and increased beam size. An absorber capable of trimming the sides of the damping wiggler beam will be mounted on the outlet of the bending magnet vacuum chamber immediately upstream of the Front end. This absorber is required to trim the beam from ±2.6mrad down to below ±1.7mrad in order to allow it to pass the sextupole and quadrupole magnets at the upstream end of the storage ring section four girder assembly. A maximum drift pipe size of 1.75" OD is allowable in this area.

The Front End Fixed aperture mask will be constructed as two masks in order to simplify manufacturing of the assembly. When trimming the beam from 3.4mrad down to the specified 1.1mrad, the mask will absorb 55kW of power. 60cm of length at a 1.6 degree angle in the vertical direction and 3.9 degree angle in the horizontal direction is required to keep the water cooled Glidcop surface below 315°C.

The absorber is cantilevered from the upstream flange to allow thermal expansion during bakeout. A formed bellow will be mounted between the masks to allow for alignment and thermal movement during bakeout.

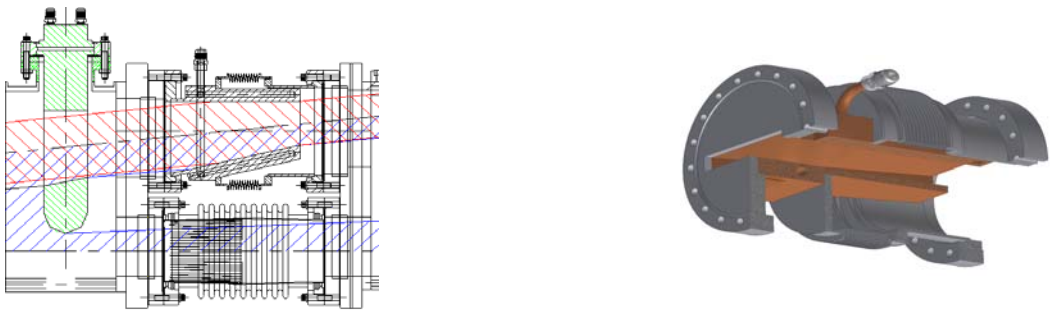

Fig. 8. Principle of the Glidcop wiggler absorber.

In Fig. 9, the thermal calculations show a peak power density ~ 200W/mm^2 at the mask, corresponding to a peak temperature ~315 °C.

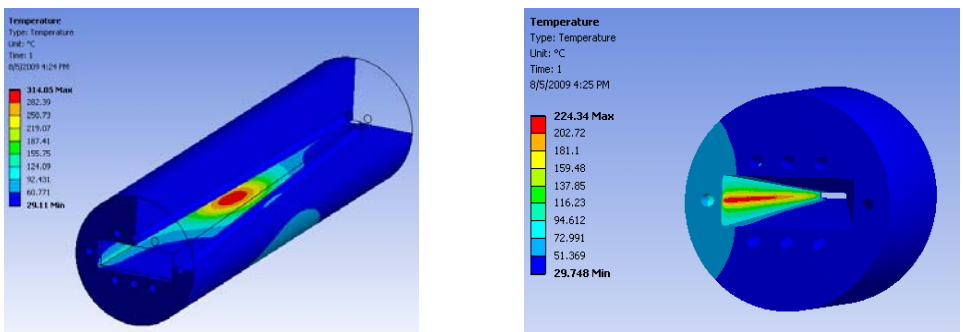

Fig. 9. Thermal calculations on the glidcop mask. (Courtesy of V. Ravindranath)

A pair of white-beam X-Y slits is located immediately down stream of the second XBPM, to further reduce power loads and reduce the angular acceptance, if required. These slits will increase in length and aperture in order to accept the damping wiggler beam. In addition to the increased size of the Glidcop slit bodies the stages supporting the slit assemblies require larger horizontal strokes.

The Photon shutter length will be increased from 20cm for an Undulator Beamline to 30cm and the horizontal aperture will increase from 20mm to a minimum of 39mm. The same actuator and position sensors will be used as on the Undulator front ends to reduce spare part requirements.

The Lead collimator length does not change but the horizontal aperture increases from 20mm to 36mm.

The safety shutter aperture will be increased from 21mm to 38mm. In addition to the primary aperture the edge welded bellows will be increased in size to 1.5” ID. Prior to final design of the damping wiggler safey shutter, cycle tests will be completed to confirm the fatigue life of the larger bellows.

Preliminary Front End X-Ray tracings have been developed for the Damping Wiggler Beamline to confirm the apertures and locations of the various front end components. The horizontal Ray tracing is shown in Appendix 2.

The effect of vertical aperturing on the overall spectral distribution and power output is shown in Fig. 11.

2.4 Optical Layout

The layout of the beamline consists in two branches and three endstations (see referenced drawings in Appendix 2).

- The first endstation will allow high energy powder diffraction studies to be conducted. A range of sample environments will be provided, and the emphasis will be on maximizing the throughput of the station; a robot will be included to assist with this and software developed for on-line data pre-analysis and quick assessment of the data. The data collection strategy and the continuation of the experiment need to be continuously guided by the on-line fast data-assessment.
- The second in-line endstation is for ´long setup time´ experiments. Beam will be delivered to the hutch, but the endstation is not fitted out within the Project scope. Much equipment for this station is expected to be transferred from NSLS and/or purchased with funds and grants from other sources.
- A parallel operating fixed energy side station for pair distribution function (PDF) experiments at ~80keV will be constructed. This equipment is not part of the present project scope either.

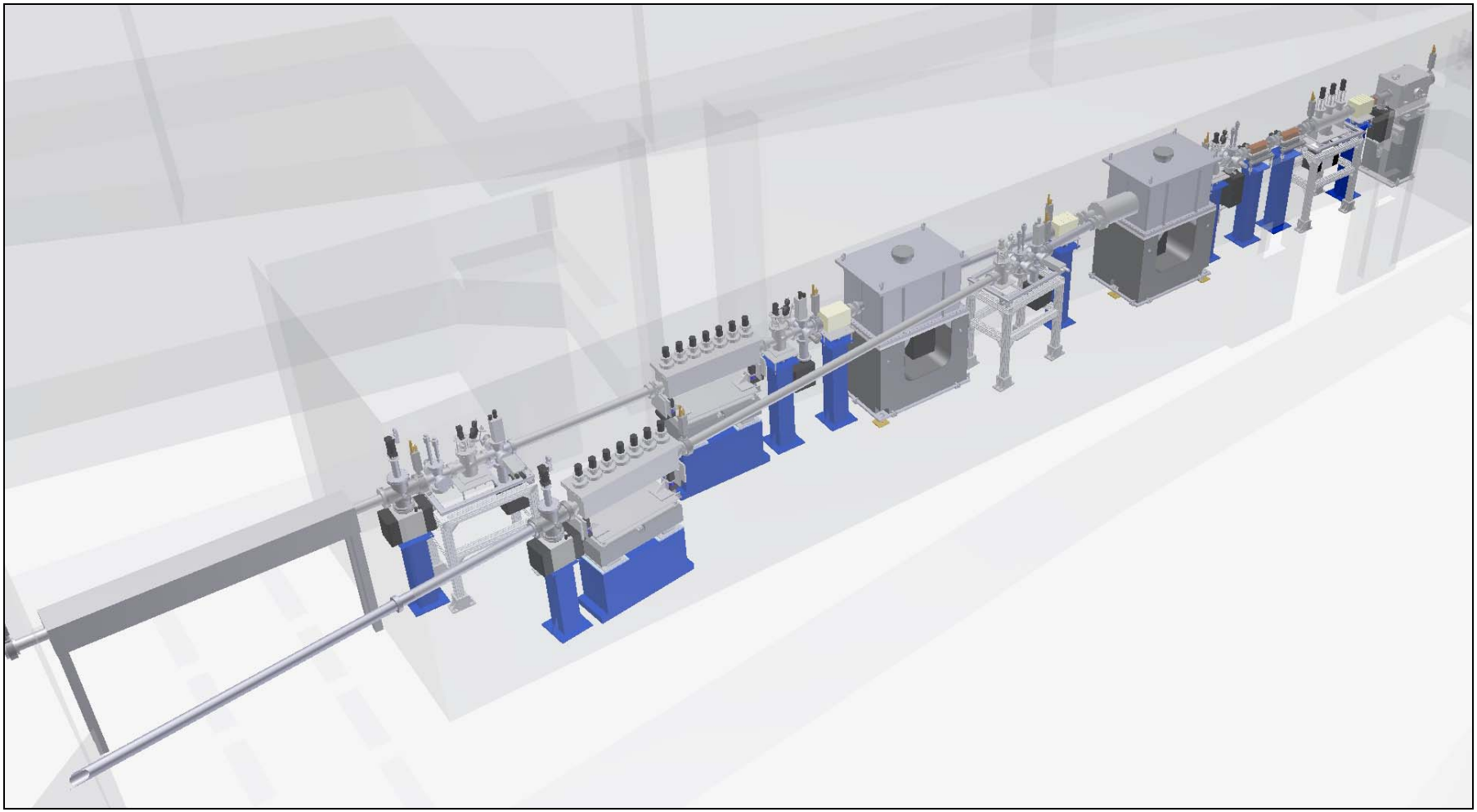

Fig. 10a. Conceptual layout for the powder diffraction beamline FOE.

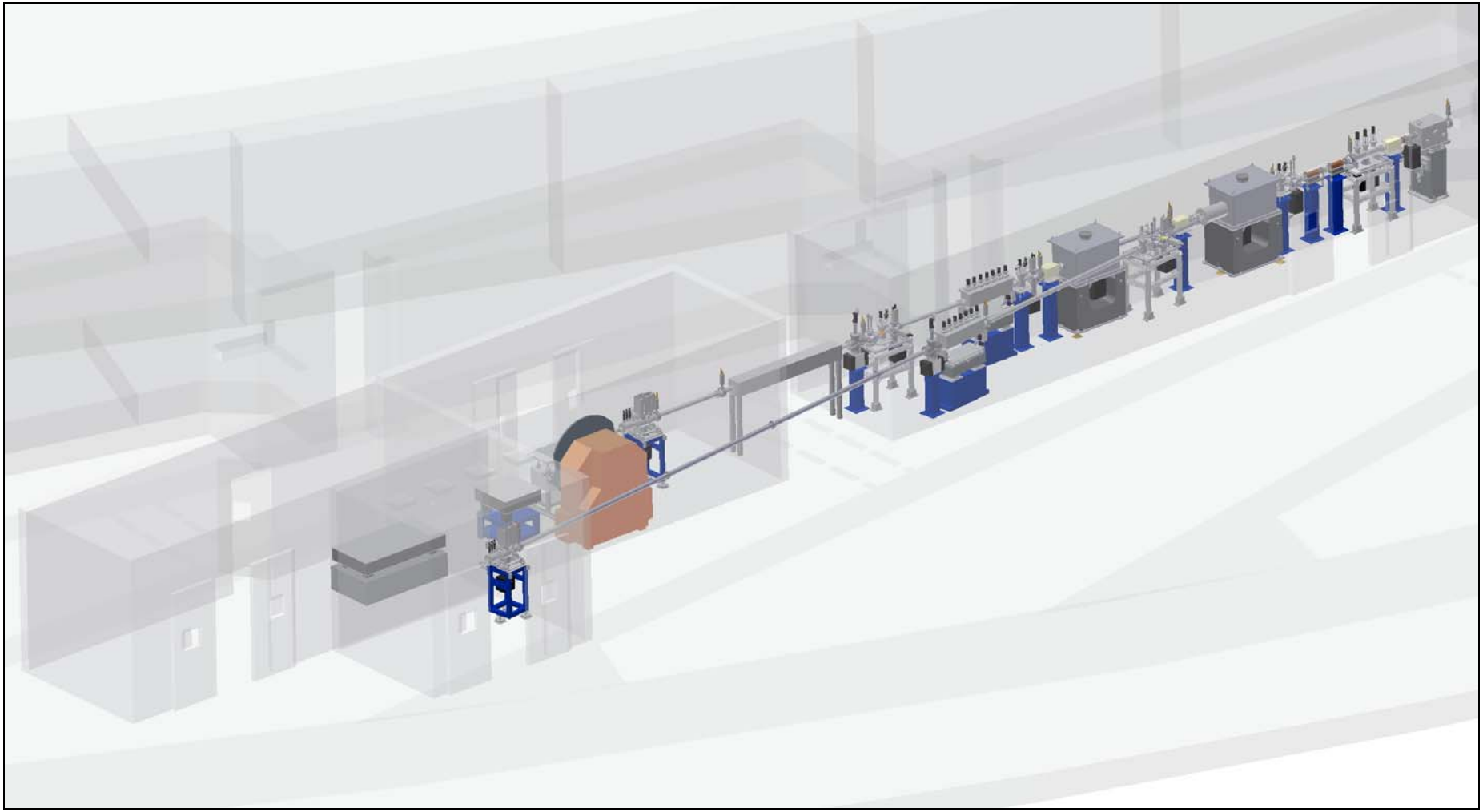

Fig. 10b. Conceptual layout for the powder diffraction beamline: FOE and all three endstations.

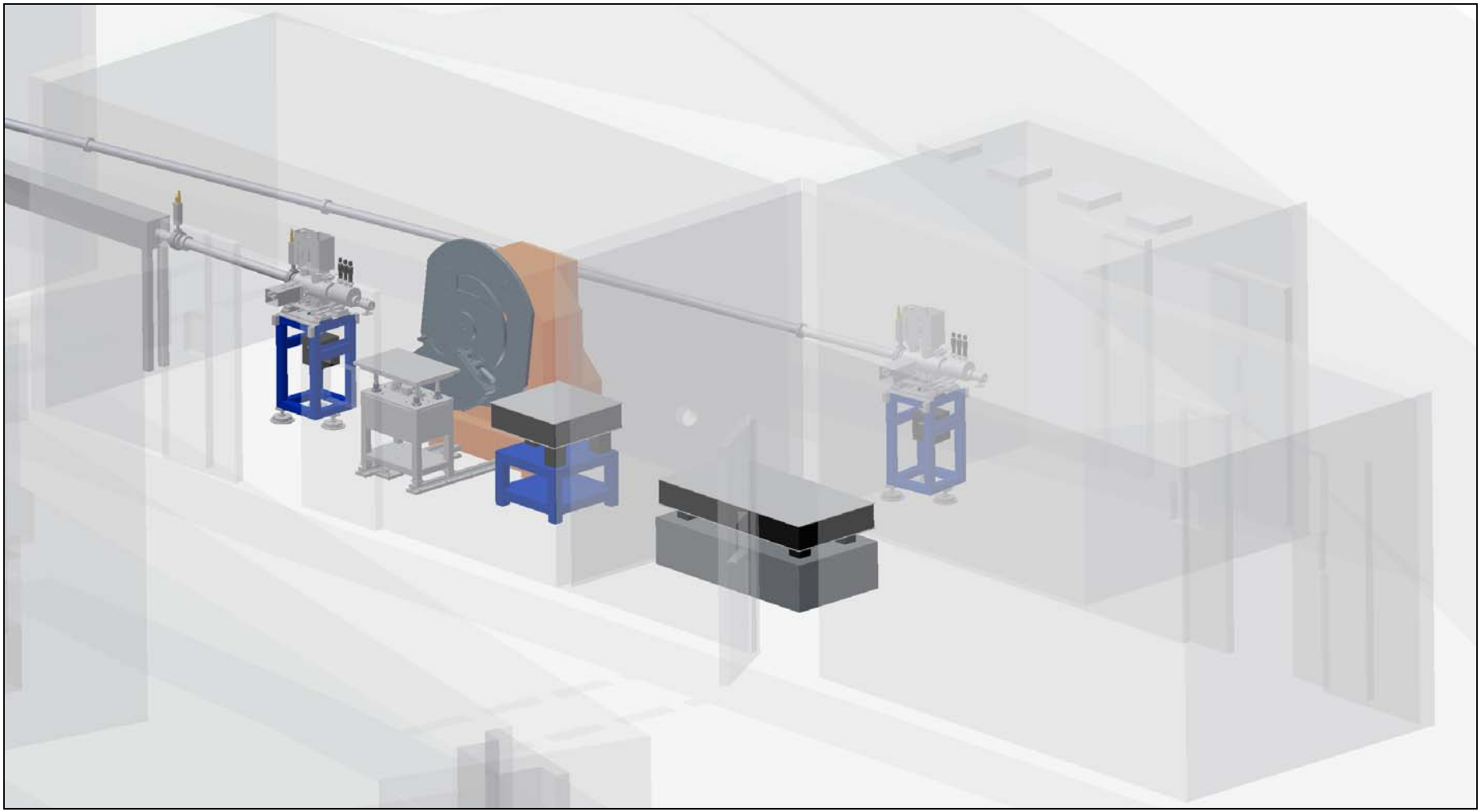

Fig. 10c. Conceptual layout for the powder diffraction beamline endstations.

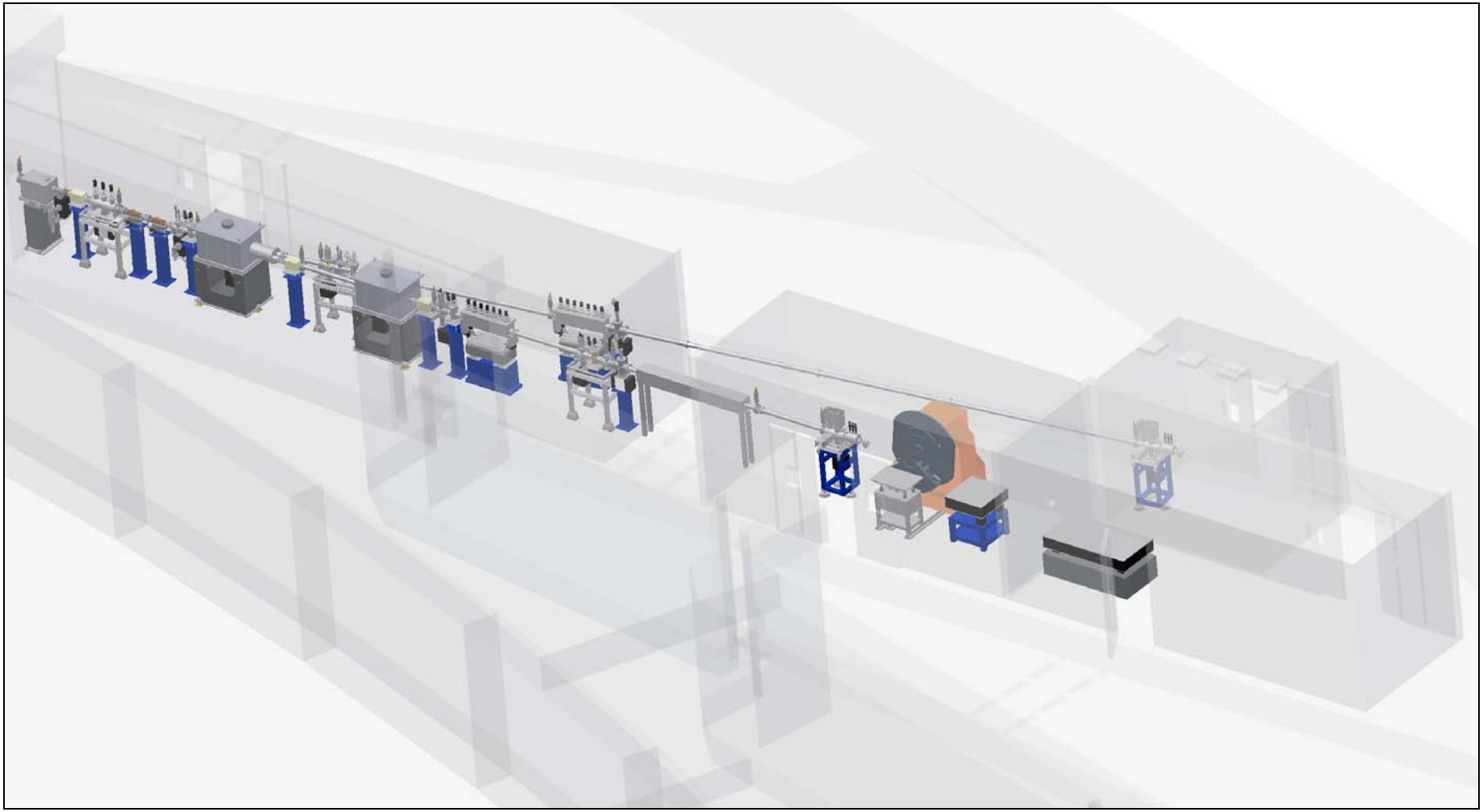

Fig. 10d. Conceptual layout for the powder diffraction beamline.

2.4.1 Main Branch

The upstream part comprises: the high-heat-load filter assembly combined with white beam slits. A single-bounce Laue monochromator, deflecting the beam sideways toward the PDF station, and a double Laue crystal monochromator (DLCM) operate simultaneously in the FOE. The DLCM geometry is based on proven technology used at NSLS at X17 and X7B (see section 2.6). The goal of the DLCM is to produce an horizontal focus with sagittal focusing around a photon energy of 40-60keV, and to deliver high flux in a small focus (less than 0.5x0.5mm^2) for small samples. The bent Laue system provides over an order of magnitude more flux, for lattice strain increases the integrated reflectivity by 1-2 orders of magnitude compared to perfect crystal. The anticlastic bending preserves a reasonable energy-resolution and increases the photon flux, given that all rays make the same incidence angle with respect to the crystal planes (the so-called Rowland condition). For many experiments, with a vertical scattering plane geometry, a beam divergence of the order of 0.1-0.2mrad at the sample and a 10^{-3} energy spread will be tolerable. Refractive optics is placed downstream and designed to either collimate or focus the beam in the vertical direction.

2.4.2 Side-Branch

A horizontally focusing Laue single-crystal monochromator produces a larger photon energy bandwidth which is related to the horizontal divergence of the beam (polychromatic focusing). The bandwidth then can be tuned by selecting an appropriate horizontal aperture. For a combination of good energy resolution and good focusing, a horizontally focusing Bragg monochromator would be better. The side-bounce monochromator will operate at a fixed nominal energy, typically 80keV. The Laue monochromator design has the option of implementing more than one crystal reaching different energies.

2.4.3 Sector Layout

The conceptual layout for the NSLS-II powder diffraction beamline is shown in Fig. 10 and in Appendix 2. The optical components are listed in Table 4 in section 2.6. Distances from the source are shown.

2.5 High Heatload Optics

Most of the thermal power of the wiggler source inherently is with the low energy spectrum (50% lies below the critical energy of 10.8 keV). *Reduction of heat load needs to be carefully considered*, addressing earlier requests from advisory/review committees for reduced technical risk. A lower power will always improve the performance of white beam optical components such as the Laue monochromators. In addition to severely *aperturing* and *filtering* the incident beam, appropriate cooling needs to be considered and integrated in the design of the white-beam optical elements (see section 2.6):

- the single Laue-crystal monochromator (section 2.6.1)
- the double Laue-crystal monochromator (section 2.6.2)

Fig. 11 shows the variation of the flux outputs at 50keV and 80keV as a function of the vertical opening, versus the total power output. It basically reflects the dependence of the vertical distributions on the x-ray energy. The nominal mask aperture is 1.1mrad × 0.22mrad, with the option to reduce the vertical aperture using the white beam slits in the FOE. A 0.22mrad vertical aperture of the mask lets all the 50keV photons through, given that the FWHM of the flux vertical distribution is 0.116mrad. A larger aperture increases the total power, but not the useful flux at 50keV. At 80keV, the useful vertical aperture is ~0.13mrad (FWHM of the flux vertical distribution is 0.09mrad). The horizontal aperture can usefully be reduced in order to keep the beam footprint on the crystal to a reasonable size.

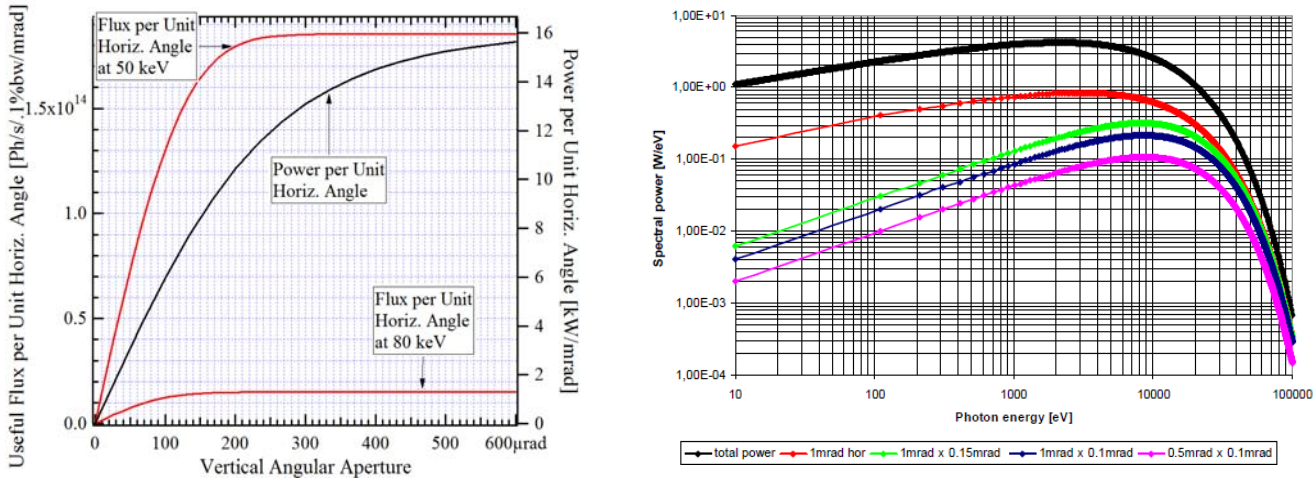

Fig. 11: (left) The variation of the flux outputs at 50keV and 80keV as a function of the vertical opening, versus the total power output; (right) The variation of the spectral power versus the aperture. The total power is: 65kW (full); 16.7kW (1mrad horizontal); 10kW (1x0.22mrad^2); 8kW (1x0.15mrad^2); 5.7kW (1x0.1mrad^2); 2.9kW (0.5x0.1mrad^2).

In hard x-ray beamlines, one typically uses a beryllium (Be) window to separate the beamline vacuum from the machine vacuum. Such a window has also the advantage that it absorbs a fraction of the unused low energy x-ray spectrum, therefore reducing the overall power on the downstream components. The 30x5x0.25mm^3 beryllium window is supported on an absorber with tapered walls, in a similar design as the FE mask. However, in a wiggler beamline such as NSLS-II DW 90 described in section 2.2, the calculation of the absorbed power indicates that a Be window in the direct white wiggler beam would simply fail: considering that the incident power is 10kW and the peak power density is 6.3W/mm^2, the calculated peak temperature in the Be window is at 890°C!

Due to carbon high thermal conductivity and mechanical stability, carbon foils are typically used as a protective filter material in front of the Be window. Our approach is to design a filter assembly that can be safely used to protect the vacuum isolation window, and that reduces the power levels on the optical components. Considering that the maximum acceptable temperature for Be is 100°C, the pre-filter is designed for reducing the incident power on the window by a factor of ~10. The upfront filters need to be very thin. 5µm of pyrolitic graphite absorb ~450W and the resulting peak temperature in the graphite foil is ~1160°C. As a first approximation, assuming the power absorption is kept constant in each foil, 20 foils are needed to reduce the incident power on the Be window from 10kW down to 1kW.

The current design of the pre-filter assembly is very similar to the setup already in use at several beamlines at NSLS (see thermal calculations in Appendix 4). It consists of a water-cooled frame that holds the different filters. The radiation-cooled foil is held in a tantalum frame, since it must withstand the extremely high contact temperature, and will become hot itself. The power then is dissipated into the surrounding environment and is absorbed by a water-cooled OFHC copper surface positioned around the tantalum frame. PT100 temperature sensors and IR pyrometers will be installed and interlocked. The final carbon filter combination has to be realized with a larger number of filter foils and a combination like the following one is a possible solution: 5 / 5 / 5 / 25 / 25 / 50 / 50 / 100 / 135 / 300 / 300 / 500 / 500 / 1000 / 1000 / 1000µm. The power density on the first foil is critical, while heat conduction and physical integrity under thermal stress limit the thickness. In case the first foil fails, the subsequent foil needs to hold the same power and should have a similar design.

As shown in Fig. 12, a set of carbon filters with a total length ≈5mm, located in the FOE, significantly reduces the heat load while decreasing the photon flux only by 19% and 17% at 50keV and 80keV, respectively.

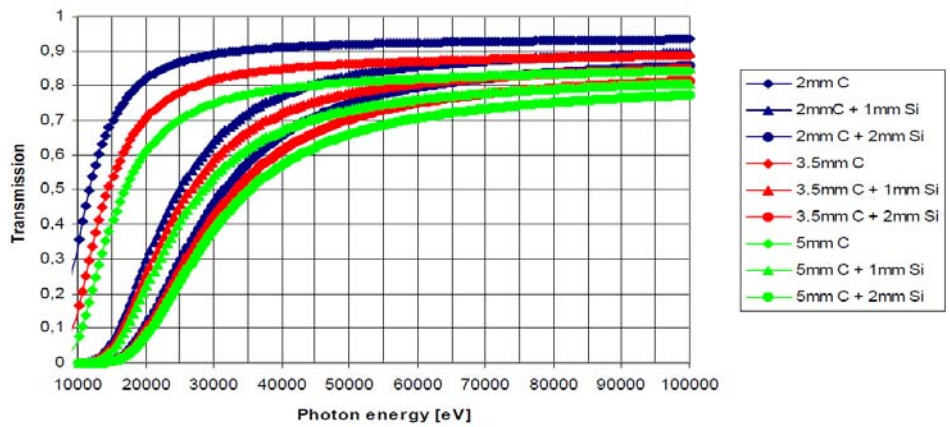

Fig. 12. Transmission of various filter combinations at the powder diffraction beamline.

After the pre-filter, the beam needs to be further attenuated to reduce the total incident power to a sustainable level (~200W). A combination of 5mm carbon, 0.25mm beryllium (vacuum isolation window) and 8mm silicon yields levels of absorbed power less than 30W that become manageable for white-beam x-ray optics. The photon flux changes by 64% and 46% at respectively 50keV and 80keV (see Appendix 4). The proposal for this beamline is to use one more fixed filter in a conservative approach for protecting the downstream optics, and one filter system that leaves the option of tuning the attenuation factor depending on the experimenter's needs. The attenuation must be adjustable in certain cases, for instance in the small beam operation mode or in case work at lower energies is required. The design of the first fixed filter, as in operation at ESRF-ID15, could consist of a water-cooled bulk rotating SiC disk. The second filter assembly consists in a controllable attenuator design and carries silicon foils of 2mm thickness each. This unit allows tailoring the power load on the optical elements to the right level of operational mode of the beamline. The water-cooled mounts are motorized and attached to a pneumatic drive.

2.6 Major Components

Table 4. The various components in the conceptual layout of the powder diffraction beamline.

Components	Distance from Source (m)
1. Front End Assembly (see appendix 2)	
2. Gate Valve (downstream of ratchet wall)	26.8
3. Pre-filter Assembly (graphite foils)	27.3
4. Beryllium insulation window	28.0
5. Bremsstrahlung Collimator	28.1
6. Second filter unit: limits the power load on the downstream optical components	28.9
7. White beam X,Y slits	29.3
8. White beam XBPM	31.0
9. White beam Fluorescent CVD screen	31.1
10. Horizontally diffracting monochromator (single Laue crystal): serves the side-branch for high-Q measurements	32.0
11. Sagittally focusing double-crystal Laue monochromator: wavelength selection, with the required band-pass	35.9
12. Bremsstrahlung stop	36.7
13. Monochromatic X,Y slits	37.5
14. Phosphor screen	37.6
15. Proposed location for 1D CRL: vertical divergence and demagnification tuning	38.5

16.	Monochromatic X,Y slits	40.8
17.	Fluorescent screen	41.1
18.	High precision BPM	41.4
19.	Safety shutter (monochromatic beam)	41.7
20.	End of FOE	
21.	Transfer tube, shielded, FOE to ES1	
22.	Hutch, EndStation 1	44.8
23.	Provisional place for second monochromator (for high-resolution operation mode)	45.1
24.	High resolution monochromatic slits	46.9
25.	Beam diagnostics, fluorescent screen	47.1
26.	Cartridge assembly: pinholes, filters, diode	47.5
27.	Exit window	47.6
28.	Ion chamber	47.8
29.	Multi-modal diffractometer in ES1 (white beam operation allowed)	48.9
30.	Support table for detectors	50.5
31.	Hutch, EndStation 2 (dedicated to long setups)	
32.	Provisional place for secondary focusing optics, used in conjunction with the CRLs	53.5
33.	Refractive Optics in branchline: 2D focusing	40.1
34.	Transfer tube, FOE to ES3	
35.	PDF side-banch station operating at 80keV (ES3)	

See referenced drawings in Appendix 2.

2.6.1 Horizontal Deflecting Side Bounce Monochromator

Horizontally focusing monochromators have been frequently used in the past (ESRF, APS, Spring8) to benefit from sources with a large horizontal divergence, like a bending magnet or a wiggler. The target photon energy for the side-bounce monochromator is beyond 80keV, while the Bragg angle will be almost fixed around 7.5 degrees (10% tunability) by the beamline geometry. Such a requirement implies the use of a high order reflection.
At the high-energy diffraction beamline at the APS, sector 11, there have been studies on horizontally diffracting Laue and Bragg monochromators [1]. A bent Bragg diffracting crystal is most suited to focus while preserving a narrow bandwidth of 10^{-3} [1]. However, such a crystal becomes very long at such a shallow angle, and it would not be practical to accept more than a 10mm wide beam (which represents a horizontal acceptance of only 0.3mrad).

In the case of Laue diffraction, the small Bragg angle is not a geometrical challenge any more: the length of the beam footprint on a Laue crystal is small and insensitive to energy. Although crystal bending preserves the natural bandwidth of the crystal to some degree while focusing a divergent beam, a white beam of large divergence on the monochromator typically implies a large energy band pass. As a consequence the bandwidth is much larger than the one obtained in Bragg diffraction. For instance, a beam divergence of 1mrad at a Bragg angle of 4 degrees produces a bandwidth of 10^{-2}. This bandwidth can be reduced to 10^{-3} when reducing the divergence to less than 0.3mrad. Appendix 5 shows our preliminary calculations. The monochromator is focusing on the slits located before the CRL assembly along the branch line. This forms a secondary source, which is re-imaged by the refractive optics at the sample position 14m downstream in ES3.

The proposed design of the monochromator assembly will ultimately need stability and reliability. The side-bounce crystal and mechanics will sit in a (UHV) vacuum vessel. A picture of a side-bounce monochromator from ACCEL is shown in Fig. 13. There is the possibility of implementing more than one crystal, leaving the choice of two

different pre-aligned crystal reflections for different energies. In such a case, one must consider a translation stage to swap between different crystals. Depending on the cooling design, that can be either a horizontal stage, or a vertical stage. On top of such translations we propose to build the rotation stages for theta (coarse), roll (coarse), and pitch (fine) (see table 5).

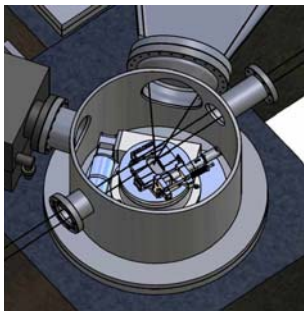

Fig. 13. CAD drawing of a side bounce monochromator. ® ACCEL-Bruker

Table 5. Possible Adjustments for the Horizontally-Focusing Single-Crystal Laue Monochromator. (Bending adjustments are not shown in this table.)

Movement	Range	Resolution	Repeatability
Whole optic assembly:			
Transversal (Y)	150 mm	≤ 0.1 mm	≤ 50 µm
crystal units:			
Roll rotation	-10 – 10°	≤ 10 µrad	≤ 20 µrad
Bragg rotation (θ_{coarse})	Full turn	≤ 10 µrad	≤ 20 µrad
Bragg rotation (θ_{fine})	± 50 µrad	≈ 0.01µrad	≈ 0.06" (uni-directional)

NSLS X17A side station (currently under design) is due to operate at 75keV and will be using a Si(311)<511> Si crystal ($\Delta E/E \approx 10^{-3}$ and angle deflection ≈7.4°). The 3mm × 3mm beam is expected to be focused to <0.5x0.5mm^2, using both the sagittal and the meridional bendings of the crystal mounted on a specially-designed two-axis bender. A silicon crystal on a cryo-cooled Glidcop bender (incident power is 40W) is being implemented at ESRF-ID24 (energy-dispersive EXAFS) with a 30:1 demagnification at 7keV. PETRA III (beamline P07) is also considering the horizontally deflecting Laue geometry for energies > 60keV [2]: the diffraction efficiency and bandwidth are controlled by a silicon crystal with either a Ge composition-gradient or a thermal gradient .

2.6.2 Sagittally-Focusing Double-Crystal Laue Monochromator

Sagittal focusing using Laue crystals was pioneered at NSLS [3-6]. The concept is shown in Appendix 5, and is increasingly used at high energy x-ray beamlines [7]. The focusing capability is similar to that of sagittal focusing by a Bragg crystal, except for a factor related to the asymmetry angle. This monochromator concept is very attractive at high energies for its flux, energy resolution, tunability and in-line-geometry properties. The good performance is imparted to some compensation effect whereby the second crystal significantly undoes the substantial brilliance degradation of the first crystal. In relaxing the bend radius of the first crystal, one finds an optimal setting where a much closer compensation occurs [8, 9].
From the current beamline geometry and distances, the demagnification ratios typically are 2.8:1 (ES1) and 2:1 (ES2), which would then give a theoretical spot size of ~60µm to ~100µm FWHM Ve.

From a first evaluation by Z. Zhong using crystal cuts with an asymmetry angle of 35.3°, it seems that a Si(311) reflection from a <100> crystal would be a good candidate at 80keV. A Si(311) reflection from a <511> crystal would be a good candidate for ≤ 50keV (see table 6). The resulting bending radii are feasible and a fixed beam

vertical offset of 20mm or more is possible. The exit beam offset has to be large enough (≥ 20mm) to provide enough clearance for bremsstrahlung shielding that is needed for personnel safety. Table 6 shows the expected flux and resolution depending on the choice of the diffracting lattice plane, crystal orientation, crystal thickness and crystal bend.

Table 6. Expected Flux and Resolution at NSLS Beamlines (Z. Zhong).

	(111)<100>	(311)<100>	(311)<511>	(111)<511>
thickness (mm)	0.4	0.4	0.6	
bending radius (m)	0.4	1.3	1.0	0.6
$\Delta E/E$ (10^{-3})	2.0	0.2	1.2	0.4
Flux (s^{-1})	5.4e+10	2.0e+09	5.6e+09	6.7e+09
		X17B1	X7B	

As seen in Fig. 14, the conceptual design consists of two pre-aligned crystal mounts with appropriate offset angles for operation. Starting from these positions, a fine tuning is available for the second crystal. The reduced Bragg angle tuning is maintained through a longitudinal translation of the second crystal having a linear attachment arm to the first crystal.

Fig. 14. NSLS Laue DCM designed by Z. Zhong.

The two sets of crystals will be sitting inside a UHV chamber, with a long lateral translation. Discussions with vendors even assume design the Laue monochromator for two or three energies, with lateral translation of crystals. It may be sensible to have one “central” setup with full tunability in bending, and side holders on kinematic mounts for “fixed” bending crystals with small adjustments possible (±5 keV). Interestingly, a single crystal bent and optimized for 80keV in the second downstream station will also focus at a lower energy in the first hutch, without changing the bend radius but only the Bragg angle.

Table 7. Possible Adjustments for the Sagittally-Focusing Double-Crystal Laue Monochromator. (Bending adjustments are not shown in this table.)

Movement	Range	Resolution	Repeatability
Whole optic assembly:			
Transversal (Y)	200 mm	≤ 0.1 mm	≤ 50 µm
2nd crystal units:			
Longitudinal (X)	300 mm	≤ 0.5 mm	≤ 1 mm
Roll rotation (χ_1)	-10 – 10°	≤ 10 µrad	≤ 20 µrad
Bragg rotation ($\theta 1_{coarse}$)	-5 – 35°	≤ 10 µrad	≤ 20 µrad
Bragg rotation ($\theta 1_{fine}$)	± 50 µrad	≈ 0.01µrad	≈ 0.06" (uni-directional)
(rotating table for the 1st crystal and cross links between the two crystals)			

As outlined before, the monochromator cooling should be carefully considered. Simple side-clamp water-cooling has shown to be inadequate through finite element analysis (FEA, see Appendix 5). Other simple methods (e.g., immersed in an In/Ga bath as in the designs at APS BESSRC CAT and ESRF ID11) are being considered before using much more demanding cryo-cooling techniques. Cryo-cooled Laue-Laue monochromator operates at APS 1-ID [7]. Similar principles could be used for XPD, if compatible with sagittal bending. Gravity fed cryocooling probably is a low-cost, low-technology, and probably an effective alternative for handling the temperature rise at the monochromator. The large acceptance (~100µrad) of the bent crystal is also relatively forgiving regarding the cooling efficiency.

In addition, the present layout is following the flexible approach taken at beamline APS 1-ID for achieving higher energy resolution, when necessary. Keeping the high resolution performance requires a low energy band-pass, typically 2×10^{-4}. This is not easily achievable with a monochromator in the Laue geometry. The current proposal is to fit the beamline with a channel-cut monochomator in ES1, which can be translated in and out of the beam. The large-bandwidth double-Laue monochromator (in the FOE) is thus followed with a high-energy/resolution monochromator (in ES1). Owing to the small (a few microradians) vertical angular acceptance of the high-resolution flat-crystal system, the beam divergence needs to be reduced by placing some collimating optics between the two monochromators (see description of the CRL in section 2.6.3). This method keeps the white beam optics fixed, and permits the subsequent high-resolution system to operate in a stable fashion without thermal load and in a more convenient room environment, where it can also be easily adapted. The monochromator at APS 1-ID consists in a four-reflection Si(111) crystal system resembling two channel-cuts in a dispersive arrangement, reducing the bandwidth to less than 10^{-4}. Another possibility under consideration is to keep the option of an additional set of unbent crystals to gain back the 10^{-4} resolution.

2.6.3 Focusing optics

High energy focusing with mirrors is extremely difficult due to the very small angle of reflection. Efficient focusing of hard x-rays using diffractive optics such as Fresnel zone plates (FZP) is limited by the ability to manufacture diffracting structures with small outermost zone width and large thicknesses. Stacked FZP or sputtered-sliced FZP can be considered, but refractive optics prove to perform better in the high energy range [10].

The purpose of one-dimensional compound refractive lenses (CRL) at this beamline will be to either vertically collimate or focus the beam at the sample. CRL are being used at other high-energy x-ray beamlines at the ESRF [11] and APS [7,8]. High energy x-ray operation overcomes the main weakness of the CRL, i.e. the attenuation of the beam through the CRL is no longer critical although a large number of lenses is required to accumulate a significant focusing effect. This relaxes the constraints on the fabrication of the lenses. At very high photon energies, the refractive index is small and therefore the preferred choice of material is silicon or aluminum instead of beryllium, or a combination of both. Approximately 15% of the available flux is absorbed at 50keV and 80keV through 5mm of Be.

Commercial CRL of high quality are available. Such lenses are shown in Fig. 15 from the Technical University of Aachen, Prof. Dr. Lengeler. Such CRL are simple to align, very stable, immune to vibrations and relatively forgiving for misorientation errors. It is recommended to use guard slits in front of the samples to avoid tails from imperfections (blurred focus etc.) and to minimize small-angle scattering halos.

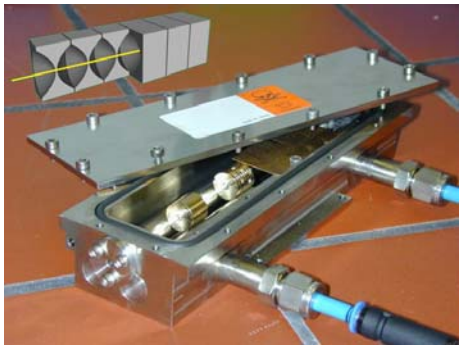

Fig. 15. Photo of the commercially available CRL setup of Prof. Lengeler, University of Aachen.

A tunable x-ray focusing apparatus based on CRL has been recently designed and tested at the ESRF (referred to as a transfocator [11]). By varying the number of lenses in the beam, the energy focused and the focal length can be varied continuously throughout a large range of energies and distances, e.g. focusing 50keV x-ray beam and partially collimating the 80keV photons. At ESRF-ID11, the transfocator is used either as a stand-alone instrument in both white and monochromatic beams to vertically focus, pre-focus or collimate the beam, or in conjunction with another focusing element downstream (CRL or multilayer mirror). Substantial gains in flux ($\geq 10^4$) are observed. In addition, the CRL can deliver a vertically-collimated beam, instead of a naturally diverging beam (0.1-0.2mrad), which better matches the acceptance of some secondary optics downstream (ES1), including a high-resolution monochromator or a secondary focusing device.

The current proposal is to use a similar design after the monochromators, consisting of highly flexible arrangements of pneumatic vertical actuators supporting a variety of cartridges containing filter foils, pinholes and masks, Al and Be lenses. The CRL are key components of the beamline which offer flexibility and different operational modes, without too much increasing the complexity of the optical setup:

- Routine work where focal length and focal spot size can be tuned
- High spatial resolution mode: the beam is sagittally focused by the Double Laue Crystal monochromator and meridionally by the CRL. An additional set of CRL or a multilayer placed closed to the sample in ES2 will tentatively produce a focal beam size of the order of 10μm.
- High 2θ resolution mode: the beam is collimated in the vertical diffraction plane, and impinges an optional channel-cut monochromator which is placed in ES1. Both the resulting low vertical divergence and low energy band pass (10^{-4}) will contribute into the resolution performance.

Those configurations are implemented at APS and ESRF [9,11], and we believe that they can be implemented at NSLS-II, for enhanced flexibility in flux/resolution and keeping the change in the setup configuration relatively easy and automated.
However, a significant drawback is the limited horizontal/vertical aperture (~1mm), which limits the gain in flux for long-focal-length (low demagnification) focusing. Table 8 shows the reduction in overall incident power and useful flux at 50 and 80keV, respectively, assuming the overall angular acceptance is ultimately defined by a 1mm effective aperture of the CRL at 30m and not by the mask in the FE. Parabolic Al lenses of 3.5mm H × 1mm V now become available.

Table 8. Reduction in Overall Incident Power and Useful Flux.

	1x0.22mrad^2	1x0.03mrad^2	0.03x0.22mrad^2
Total power (kW)	11	1.8	0.04
Flux (10^{14} ph/s/.1%bw) at 50keV	1.8	0.45	0.06
Flux (10^{14} ph/s/.1%bw) at 80keV	0.15	0.05	0.005

Alternatively, a 1m long Pt coated mirror at a glancing angle of 89.9427° (critical energy = 80keV) would ensure a good reflectivity and could also capture 0.03mrad of the vertical fan. Since it will be placed after the monochromator, a simple design (no heat load) can be considered with a substrate made of glass or metal. Multilayered mirrors $(W/B_4C)_{300}$ with periods as small as 2nm could offer an even better option, considering their higher incidence angle.

2.7 Summary of Beamline Performance Specifications

Powder diffraction experiments will be performed in both the high-resolution (angle-scanning) and area (fixed) detector modes. The crystal analyzer [12,13], in use at the diffactometer in ES1, is the most demanding in terms of angular stability, since it aims to provide high d-spacing resolution and precision. The area detector mode is primarily affected by position stability. Both modes are sensitive to beam energy changes.

In the crystal analyzer mode [12,13], the critical requirement is angular stability. A typical powder peak width using an analyzer Bragg crystal is in the range of 0.005^o to 0.01^o in the 10-30 keV range, depending on the sample quality. 0.001^o is unusually good. Let us consider 0.005^o as typical. Then, the photon beam stability should be 10% of this value i.e. 0.0005^o, or 8μrad.

A related concern is the energy stability, since energy maps directly to d-spacing in a diffraction experiment. Using Si(111), its intrinsic energy resolution, $\Delta E/E \sim 10^{-4}$, sets a limit on what can be achieved. If we assume we can find centroids to a few percent of this, we end up with an energy stability requirement of at least 10^{-5}. This requires an angular stability of 1 or 2 μrad (Si(111) at 17keV has a Darwin width of 15μrad), and a monochromator temperature stability of 10°K.

All of the above arguments are directed in the vertical plane of diffraction.

The resolution using an area detector typically is 10 times lower than that using scintillation counter with a crystal analyzer, so angular stability is not the limiting case. In contrast to the crystal analyzer mode, position stability is important, since position is used as an angle analogue. If we assume a focused beamline with a focal spot of 100μm and a detector with a 100μm spatial resolution, then using the '10% rule', beam stability should be on the 10μm level. Similar arguments apply to energy stability. In this case, the spatial stability requirements are in both the horizontal and vertical directions.

3. END STATION INSTRUMENTATION

The first endstation will be ~3m wide × 7.5m long and very similar to modern, highly productive, stations at the ESRF, SLS, APS, ASP and will cater to a wide range of users interested in higher energies (>50keV). The core instrument consists of a highly accurate 3-axis diffractometer (Fig. 16): The "inner" stage will be for sample rotation, but will have a capacity of 35kg at a distance of ~200mm from the interface plate; this will allow the rotation of heavy samples with environmental cells where applicable. The interface plate is fitted with "spherolinders" (heavy duty kinematic type mountings with cylindrical rather than spherical attachments); these will allow sample environments to be swapped over easily and with minimal alignment. A Euler cradle and a x-y-z stage can be fitted on that circle, with appropriate sample positioning (metrology, alignment) and beam position monitoring. Opposite the diffractometer, a translating table can support larger loads such as large cryostats and furnaces and high pressure cells. In addition, a robot for fast and automated sample changing is recommended for high-throughput measurements for combinatorial investigation and screening purposes.

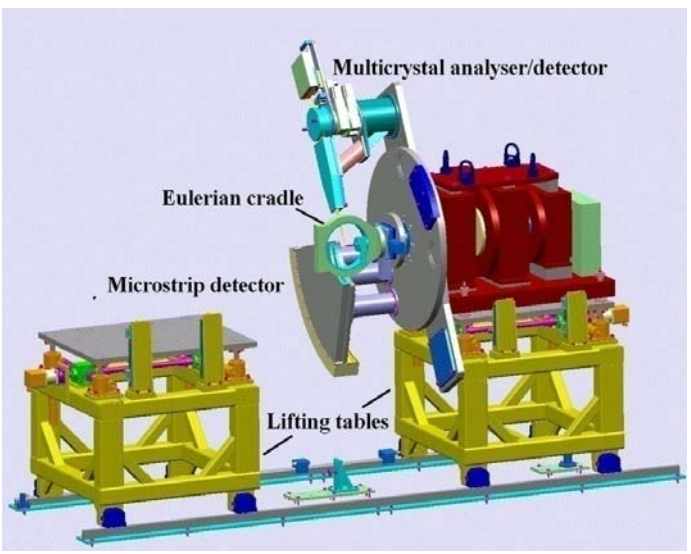

Fig. 16. Conceptual design of the NSLS-II high-energy high-resolution powder diffraction beamline. For clarity, sample environments (such as cryostats, furnaces and diamond-anvil cells) and a robotic sample changer for high-throughput applications are not included in the figure.

The second axis holds a fast read-out position sensitive silicon strip detector for in-situ time-resolved studies and remains essentially fixed. The implementation of a fast position-sensitive strip-array detector allows the real-time, microsecond timescale study of phase transitions, transformations, and catalytic reactions as a function of temperature, chemical gradients, and pressure. The third axis is essentially used to hold a multi-crystal array analyzer system that can be rotated in the vertical diffraction plane, and meant for high-resolution high-energy studies. This arrangement proves to work satisfactorily and to cover a wide range of users' needs on several PD endstations. In the present scope, it is envisaged to mount a second angle-scanning stage for scanning over the high-angle range with a medium resolution (larger angle step size and longer count time are required over the far-Q range). In this unique arrangement, both angle-scanning stages could operate simultaneously, recording complementary parts of the diffraction diagram. They will run in a continuous scanning mode, replacing the usual step-by-step "move and count" mode for better efficiency (minimal overhead). The resolution of the rotary stages and the encoder readings need to be accurate to obtain exact peak positions and reliable data. The Newport and RPI systems have the necessary resolution to enable the operation of this facility.

The most advanced powder diffraction machines now provide instrumental peak widths (FWHM) as low as <5 milli-degrees in the 10-30keV energy range, thus allowing accurate peak profile measurements and minizing the peak overlap effect. The former is essential for the study of strain, microstructure and lattice defects. The latter is required for peak indexing and peak intensity extraction (using the Le Bail approach) in structure solution. The high resolution operation is achieved using a bank of analyser crystals on the diffracted beam paths. To our knowledge, all existing designs rely on the concept developed at the ESRF by J-L. Hodeau et al [12] and use Bragg crystals.

This cannot be transposed to the present case. High energy diffraction imposes very shallow Bragg angles (extended footprint of the impinging beam on the analyzer crystals) and higher shielding and collimating for reducing the cross-talk and noise level. Such a stage would need to accommodate long Bragg crystals, and x-ray tracing shows that it would be extremely difficult to keep the design compact and light-weight. Moreover any energy change will cause important drift of the sample-diffracted beam impact point over the surface of each analyzer crystal, making the alignment extremely difficult [13].

The DOE review committee of last June recommended that novel detection schemes such as Ge Strip detectors and Laue Crystal Analyzers should continue to be explored. These issues are addressed in the following sections.

3.1 High Energy X-ray Detectors

Powder diffraction often requires different data collection strategies, and make use of such detectors as:

- High count-rate high-energy scintillation counters
- upgrade from baseline Si-based strip array (e.g. Mythen, XSTRIP) to Ge-based detectors
- MAR 345
- CCD–fiber tapers are now routine e.g. Frelon ESRF
- Pilatus II, MediPix, XPAD (PAD with in-pixel processing)
- Pixium (ESRF, Thales) or GE Healthcare (APS)

The route to high efficiency, high energy detectors and energy-discriminating area detectors should lead to many more exciting opportunities in high energy x-ray diffraction science in the coming years. *But the lack of detectors that perform well at high x-ray energies is a real concern and this development will noticeably impact the performance of the beamline* (see appendix 7).

3.2 High-Resolution Analyzer Stage

The overall design of the diffractometer is relatively standard, although a significant R&D effort is needed for optimized performance above 40keV. By employing a high-resolution crystal analyzer array, this new instrument will enhance the quality of the diffraction data, through suppression of the fluorescence and Compton components (including diffuse scattering). This is a prerequisite to evaluate technologically important disordered materials. Due to the inherent small instrumental (and source) broadening, the high resolution of the crystal array will enable the measurement of accurate peak-profiles, thus allowing the investigation of strain, lattice defects, and micro-structure.

Low Bragg angles at short working wavelengths make it less suitable to use an array of parallel post-sample crystals in the reflection geometry. The analyzer stage would better work in the transmission geometry using Laue crystals. To our knowledge, such a design does not exist nowadays [13]. A solution is proposed by Siddons et al. in reference [13] as a relatively simple 16-element crystal analyzer based on a single monolithic piece of Si (Fig. 17), elastically bent in a pseudo-Rowland circle geometry and combined with a compact 16-channel pulse-counting detector. This detector could be a custom multi-element germanium or CdZnTe detector, made inhouse by the NSLS Detector Development Group. This particular device requires some x-ray tracing simulation and prototype-testing.

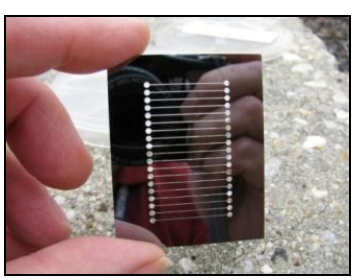

Fig. 17. The Laue crystal array from [13]. The rectangular slats in the center of the crystal are the diffracting elements. The wide side plates are the elastically defornung part. The crystal is clamped at top and bottom, and a bending moment applied to curve the object into a segmented cylinder. The strain induced by the bending is isolated from the diffracting elements by the small cross section of the connecting fillets.

3.3 Software Development

More and more, users expect to find a user-friendly "expert" software that insures they walk away from experiments with data sufficiently processed for analysis at their home institution. For the sake of beamline efficiency and reliability, this is desirable and achievable, provided significant software development accompanies the implementation of the endstation instruments. This includes:

- On-line quick data assessment for rapid evaluation and as an easy assistance of the user in his decisions regarding the subsequent measurements.
- Data reduction and analysis to handle the large amount of 1D and 2D data the beamline is likely to produce in the future. The user comes back home with pre-processed data and preliminary results, rather than with DVD disks of 2D raw data.

The SR user community more and more often points at data handling and data analysis as being a recurrent bottleneck for producing science from SR measurements. Therefore this particular issue should be addressed right from the start of the project conception, and should be an integrated part of the beamline design.

Table 9. A list of detectors and their requirements in terms of data storage and data rate.

Detector / station	Data production	Data rate
CMOS flat panel detector for PDF station	50MB image size, 10 Hz.	500 MB/sec
Strip detector in high throughput station	13 x 80mm modules with 125 micron strips (8320 elements) running at 1kHz	6 MB/sec
Crystal analyzer detectors	Very low data rate	
CCD for special setup enclosure	30MB image size, 1 Hz	30 MB/sec

3.4 Complementary Experimental Stations

Although not in the scope of the present NSLS-II project, the **second hutch** (~3 × 9m^2) is meant for special sample environments and long setups. The second station (ES2) will be built as large as the existing floor allows. The access and facilities will be designed to allow very flexible setups with reasonably easy changeover of experiments. It could be partially populated by existing NSLS equipment and will be able to accommodate a variety of users' designed chambers and cells using heavy-duty supports and a crane. We anticipate such a facility would also be in high demand at NSLS-II. A graded bendable multilayer system or a 2D focusing CRL may be used to focus the beam to ~10 microns for studying small samples (e.g. for high-pressure diamond-anvil cell research). This focusing optics is located relatively close to the sample position to minimize beam motion. This secondary focusing device can be used in conjunction with the "transfocator" (see section 2.6.3).

Local and nanostructure studies are often referred to by the method name, pair distribution function (PDF) analysis, or total scattering, which refers to the fact that all the scattering (Bragg and diffuse) is utilized. Hard x-rays are well suited to PDF studies of nanostructures in particular. Current approaches for studying nanostructure utilize the PDF method combined with full profile fitting structural modeling. Efforts are under way to incorporate information from complementary methods (anomalous diffraction, EXAFS, x-ray and neutron data, NMR, quantum chemistry, etc.) in a rational way when the problem is under constrained. A recent breakthrough was the first demonstration of ab initio structure solution of a nanoparticle from PDF data. However, there is still a long way to go to develop these tools to the level of confidence enjoyed by crystallographic methods. Beyond the present baseline proposal, we are considering combining the structural Q-dependent measurement with a space-resolved probe. Recently, it was shown how diffraction and the tomographic method could be combined for 3D phase imaging [14]. The PDF work can be accommodated in the **third hutch**; its instrumentation is not in the scope of the present project.

The PDF side station shall be ~3 × 4m^2. The concept for this station is based on APS beamline 11-ID-B and NSLS beamline X17A, which feature a single horizontal bounce design. A thin bent Silicon crystal in the Laue geometry will kick the beam sideways and simultaneously provide horizontal focusing, it should be noted that this is at the

expense of bandwidth, although this will not be an issue as 10^{-3} bandwidth is sufficient for PDF studies (see section 2.6.1).

- Energy needed is ~80keV (as high as possible but giving sensible beam separation).
- The CRL could be common to both branches, but there is a preference to put independent CRLs on each branch, after the individual monochromators.
- The horizontal focus is <300 microns.
- The energy will be switchable through the implementation of a double crystal setup (one on top of the other, which just translate vertically through the beam to switch over).

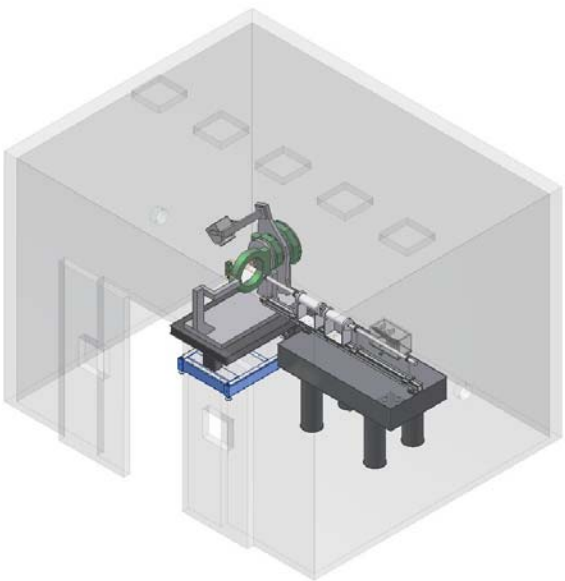

Fig. 18. Conceptual layout for a second powder diffraction beamline, downstream of the high-energy high resolution NSLS-II powder diffraction beamline. Note that this endstation is not in the current scope of the NSLS-II project.

3.5 Sample Environment

Considerable efforts will be made to ensure that a wide range of sample environments are made available to the user community. The access and facilities will be designed to allow very flexible setups with reasonably easy changeover of experiments. For easy configuration changes, we are considering the use of "towers" mounted on rail paths, instead of granite table benches: sample tower, detector tower, optics tower (filters, slits, shutter, laser, collimator,…). The user can come along with his own custom setup, and put it on the top of a heavy-duty (200kg) Huber table (rotation φ, translations X and Y, coarse and fine Z), supported on a granite base plate and motorized on rails. A variety of sample environments (not shown) are included in the budget, consisting of cryostats, furnaces, laser heating and diamond-anvil cells for high-pressure research. A typical suite of ancillary equipments on modern powder diffraction instruments includes:

- Stoe capillary furnace (T = 300 – 1700K)
- MRI flat plate furnace, (T=300 - 2000K)
- Bruker Humidity chamber (-5°C up to 75°C dew-point, T= 25 – 90°C)
- Linkam DSC (T = 77 – 870K)
- Cyberstar Hot air blower (T = RT-1300K)
- PheniX He Cryostat (T = 11 – 300K)
- ASI cryostat (T= 4 -300K)
- Oxford Cryosystem 700+ cryostream (T = 80 – 500K)

To support modularity, rapid interchange of sample environments, and extensibility in the future, instrument interfaces and software will be carefully designed and specified. The scattering from sample environments often

compromises the data quality in experiments at non ambient conditions. Tight collimation and/or small focus are necessary to minimize or totally exclude parasitic scattering from the sample environment.

Table 10. List of ancillary equipments and sample environments.

Technique and equipment	Size of equipment (typical)	Weight (approx)
HP Earth and Materials Sciences: 2000T press to give routine 50 GPa at sample.	4m x 4m plus plumbing (hydraulics) plus accessories.	2000 kg
HP Earth and Materials Sciences: Double sided laser heating (2500K) for routine experiments up to 200 GPa.	3m x 2m plus plumbing and accessories.	100 kg including laser and stand.
Catalysis cells with goniometer and detector on 1m arm.	2m x 2m plus gas handling and analysis equipment.	500 kg
Carbon sequestration and catalysis. High pressure CO2 cell.	1m x 2m plus accessories.	1000 kg including cell, rotation stages, area detector etc.
Engineering applications (white beam, fixed angle EDX, high capacity 0.5μm resolution x/y/z translating table, for scattering in the vertical and horizontal).	3m x 3m	2000 kg
Single-crystal setup concentrating on higher energy experiments and heavier loads (complements standard set up beamline proposed on adjacent BM line).	~2m x 2m	1000 kg

4. SPECIAL BEAMLINE REQUIREMENTS

Although a plethora of user-friendly ultra-high temperature, high pressure and apparatus are designed and built for the study of materials *in operando*, it is critical that the 5-year horizon to the construction of XPD be accompanied by efforts to prototype environmental chambers, and to push ahead with ever more suitably high time, angular and spatial resolution optics and detectors.

Because the beamline is intended to study materials under operational conditions, we can anticipate that most (if not all) of the 241 substances in CAA 112R, the EPA list of Regulated Toxic, Explosive, or Flammable Substances, will be used at some time - fortunately in small quantities. Many of them are involved in catalytic processes and/or semiconductor manufacturing, two key areas of beamline science. A ventilated cabinet for dangerous gas bottles is required, and the gases will be piped to the first hutch.

Many catalytic studies will involve multiple reagents. It is easy to imagine feeding a mixture of gas, gaseous hydrocarbon, and liquid hydrocarbon into a reactor. Systems to control the flows of such materials (including mass flow controllers interfaced to data collection software), as well as to monitor the composition of the products (online GS/MS, also interfaced to the data collection software) will be required from the outset. Because each experiment will have different requirements, modularity of the endstation equipment will be critical, but as much common infrastructure as possible needs to be provided to maximize the productivity of the beamline.

Table 11. List of potential catalysis applications and chemicals involved.

Reaction	Potential "interesting" compounds involved
Ammoxidation	NH_3, air, propylene/propane, acrylonitrile, acrolein (avoid flammability limits)
Partial oxidation	Butane, air (flammability limits)
Xylene isomerization	Hydrogen, xylenes, toluene, ethylbenzene, benzene, ethane/ethylene
Hydrotreating	H_2S, NH_3, H_2 (P < 5000 psig)
Offgas treating	CO_x, NO_x, SO_x, HCl, HBr
Oxychlorination	Cl_2, HCl, vinyl chloride monomer
Olefin Polymerization	Metal alkyls, metal chlorides, HCl, BF_3
Alkylation	H_2SO_4, H_3PO_4
Many reactions	H_2O (steam)
Hydrogenation	H_2, aromatic acids, acetic acid

The proximity of the Center for Nanomaterials and trends in current frontier science suggest that many experiments involving nanomaterials will be performed at the beamline. A HEPA filtration system needs to be an integral part of the endstations.

5. FUTURE UPGRADE OPTIONS

Operating the beamline with "extremely" small (1-2µm) beams, especially in the context of one of the major scientific goals to study heterogeneous samples *in operando*, opens more scientific possibilities. *1-2µm focusing is an untried technological challenge to deliver from a wiggler source*. Whilst highly desirable, this is not a design goal of the beamline: 5–20µm vertical and 20–50µm horizontally focusing are in the base design, and the 1–2µm focusing is kept in mind as a long term goal with enough room left in the beamline to accommodate possible optics (CRL, KB, ML) for this purpose in the future. The capability of delivering small beams (below 10µm) is thus being considered as part of the mature scope of the project, below the build-out of the PDF side-station in priority. The current layout keeps the option of a primary focus and slits at the first hutch position and then refocusing optics to produce a 10µm focus in the second hutch; this would be unique at these energies.

An important and unique feature of the beamline will be the ability to combine the angle-dispersive setup with energy step scans. Alternatively, we can use a so-called "pink" beam or a large energy band-pass beam. This is particularly important when the grain statistics of the sample is insufficient. This well-known sampling problem in powder diffraction impairs the diffraction intensities and introduces significant biases in the resolution of the diffraction pattern. This occurs for a non-spinning sample (as it frequently happens for a sample confined inside an environmental cell in a fixed geometry) or when the beam does not probe a sufficient number of randomly oriented crystallites. This is very common for spatially-resolved measurements using a focused beam below 10 microns size (small gauge volume) or with a poor powder or not quite a powder. Varying the energy of the monochromatic beam or using a non-monochromatic beam often helps overcome this grain problem. Combining the energy scan with an area detector will probably develop in the future years: a relevant example is shown by Wang et al. [15] in an energy-dispersive measurement, whereby the Ge solid-state detector is angle-scanned (and not at a fixed angle as usual) for covering a larger fraction of the reciprocal space.

An interesting option is to use the transfocator as a broad energy band-pass (1%) monochromator, simply using the longitudinal chromatic dispersion of the focused beam. This acts as a *longitudinally dispersive monochromator*, and will prove to be particularly useful for powder diffraction on "poor" powders, non spinning specimens, dilute or extremely small samples or time resolved work. Provided focal length is kept relatively short (a few meters), the depth of focus is sufficiently short that only a narrow band pass is focused at a given longitudinal point. At the focal point, this leads to a substantial increase in the flux at this selected energy with respect to the rest of the spectrum. The first experimental hutch could therefore be designed for accepting an in-going white beam. The desirability to

change from a monochromatic beam (as in the current baseline design) to a white beam hutch is under investigation.

6. SUMMARY

Powder diffraction has widespread scientific interest, such as in the fields of metallurgy, solid-state chemistry, nanomaterials, microelectronics, mineralogy, and the biological and pharmaceutical sciences. In addition, the study of condensed matter at extreme conditions is developing into a very rich field of research. In situ elastic scattering provides the data required to derive structure models, which is essential to systematic searches for new classes of materials and to rationalizing their desirable properties.

The proposed powder diffraction beamline at NSLS-II will be a tunable high-resolution facility with the ability to collect data at high energies (50keV-100keV), offering exceptional capabilities such as fast (milli-second) readout rates and high angular resolution on the same instrument. The high-energy x-rays will be able to propagate through environmental cells, and are suitable for powder diffraction measurements in difficult environments, e.g., stainless steel reaction tubes and high temperature capillaries. It also allows for the investigation of materials made up of high-Z components, and enable high-Q accessibility, which is crucial for atomic pair distribution function analysis and high-pressure cell research. This will be an outstanding research facility for studying the structure and kinetics of materials under real conditions, and the beamline will meet the needs of the powder diffraction user community.

This report has presented a conceptual design of the XPD project beamline. Additionally, we have described proceeding hutch ES2 and hutch ES3 build-outs in a preliminary stage of development. The beamline components are based on proven concepts. The combination of high-heat load double-Laue crystal with refractive optics is or will be used in particular at ESRF-ID15, ESRF-ID11, APS-11ID and PETRA-P07. This design proves to be a stable configuration and performs well in the high-energy range. The present proposal is adopting a similar strategy tailored to the characteristics of the Damping Wiggler source, in particular for handling the large horizontal fan.

Because of the nature of complex materials research, the scientific impact depends equally on beamline characteristics and on the existence and usability of appropriate software and special environments, and on the success with which researchers can combine data from complementary approaches (such as conventional powder diffraction and PDF).

More information regarding the experimental facilities and the standard beamline components can be found at the NSLS-II Conceptual Design Report web page.

7. REFERENCES

1 M.A. Beno, U. Rütt, C. Kurtz, G. Jennings. Synchrotron Radiation Instrumentation: Eight International Conference on Synchrotron Radiation Instrumentation, CP705, p.675, 2004, San Francisco.

2 U. Rütt, J. Heuer, H. Schulte-Schrepping. Private communication. Work based on R. Smither, K. Abu Saleem, M. Beno, C. kurtz, A. Khounsary, N. Abrosimov. Rev. of Sci. Insstrum. 76 (2005) 123107.

3 Z. Zhong, C.C. Kao, D.P. Siddons and J. B. Hastings. J. Appl. Cryst., 34 (2001) 646-653.

4 Z. Zhong, C.C. Kao, D.P. Siddons and J. B. Hastings. J. Appl. Cryst. 34 (2001) 504-509.

5 Z. Zhong, C. Kao, D.P. Siddons and J.B. Hastings. Acta Cryst, A 58 (2002) 487-493

6 Z. Zhong, C. Kao, D.P. Siddons, H. Zhong, and J.B. Hastings. Acta. Cryst. A 59 (2003) 1-6.

7 S. D. Shastri, K. Fezzaa, A. Mashayekhi, W.-K. Lee, P. B. Fernandez and P. L. Lee J. Synchrotron Rad. 9 (2002) 317.

8 S.D. Shastri. J. Synchrotron Rad. 11 (2004) 150–156.

9 S. D. Shastri. J. Almer, C. Ribbing and B. Cederstrom. J. Synchrotron Rad. 14 (2007) 204–211

10 A. Snigirev, I. Snigireva, M. Grigoriev, V. Yunkin, M. Di Michiel, S. Kuznetsov, G. Vaughan. Advances in X-Ray/EUV Optics and Components II, ed. by Ali M. Khounsary, Christian Morawe, Shunji Goto, Proc. of SPIE Vol. 6705 (2007) 670506.

11 http://www.esrf.eu/news/spotlight/spotlight85/spotlight85/

12 J.L. Hodeau, P. Bordet, M. Anne, A. Prat, A. N. Fitch, E. Dooryhée, G. Vaughan, A. Freund, SPIE Conference on Crystal and Multilayer Optics, San Diego 1998 SPIE Vol. 3448 p 353.

13 D. P. Siddons, Zhijian Yin, L. Furenlid, P. Pietraski, Zheng Li, R. Harlow. A. Freund2, SPIE Conference on Crystal and Multilayer Optics, San Diego 1998 SPIE Vol. 3448 p120.

14 P. Bleuet, E. Welcomme, E. Dooryhee, J. Susini, J-L. Hodeau, P. Walter. Nature materials 7 (2008) 468.

15 Y. Wang, T. Uchida, R. Von Dreele, M. L. Rivers, N. Nishiyama, K. Funakoshi, A. Nozawa and H. Kaneko. J. of Applied Ccrystallography 37 (2004) 947.

16 P. Suortti, S. Fiedler, A. Bravin, T. Brochard, M. Mattenet, M. Renier, P. Spanne, W. Thomlinson, A. M. Charvet, H. Elleaume, C. Schulze-Briese and A. C. Thompson J. Synchrotron Rad. 7, p.340, 2000

17 C. Schulze, U. Lienert, M. Hanfland, M. Lorenzen and F. Zontone. J. Synchrotron Rad. 5, p. 77, 1998

18 C.G. Schroer, M. Kuhlmann, B. Lengeler, T.F. Günzler, O. Kurapova, B. Benner, C. Rau, A.S. Simionovici, A.A. Snigirev, I. Snigireva. Proc. SPIE, 4783 (2002) 10–18.

19 A. Stein, K. Evans-Lutterodt, N. Bozovic, A. Taylor. J. Vac. Sci. Technol. B 26 (2008) 122

20 A. F. Isakovic, A. Stein, J. B. Warren, S. Narayanan, M. Sprung, A. R. Sandyd and K. Evans-Lutterodt. J. Synchrotron Rad. 16 (2009). 8–13

21 Jark,W., Perennes, F. & Matteucci, M. J. Synchrotron Rad. 13 (2006) 239–252.

22 E. Dooryhée, M. Anne, I. Bardiès, J.-L. Hodeau, P. Martinetto, S. Rondot, J. Salomon, G.B.M. Vaughan and P. Walter. Appl. Phys. A 81 (2005) 663.

23 P.J. Chupas, K.W. Chapman and P.L. Lee. J. Appl. Cryst. 40 (2007) 463–470

24 J.H. Lee, J. Almer, C. Aydiner, J. Bernier, K. Chapman, P. Chupas, D. Haeffner,K. Kump, P.L. Lee, U. Lienert, A. Miceli, G. Vera. Nuclear Instruments and Methods in Physics Research A 582 (2007) 182–184

25 J. E. Danielsa and M. Drakopoulos. J. Synchrotron Rad. 16 (2009) 1

26 J.-F. Berar, L. Blanquart, N. Boudet, P. Breugnon, B. Caillot, J.-C. Clemens, P. Delpierre, I. Koudobine, C. Mouget, R. Potheau, I. Valin. J. Appl. Cryst. 35 (2002). 471-476

27 P. Pangaud et al. Nuclear Instruments and Methods in Physics Research A 591 (2008) 159–162.

28 V.A. Wright, A. Blue, M. Horn, I. Johnston, E. Koskiahde, L. Lea, J. Melone, S. Nenonen, V. O'Shea, M. Rahman, P. Roy, K. Smith. Nuclear Instruments and Methods in Physics Research A 531 (2004) 56.

29 B. Schmitt, Ch. Bronnimann, E.F. Eikenberry, F. Gozzo,C. Hormann, R. Horisberger, B. Patterson. Nuclear Instruments and Methods in Physics Research A 501 (2003) 267–272

30 S. Basolo et al. J. Synchrotron Rad. (2007). 14, 151–157.

31 J-C. Labiche et al. Rev. of Scientific Instruments 78 (2007) 091301

APPENDIX 1 SCHEDULE

September 30	2009	Complete Conceptual Design Report
September 28	2010	Complete Preliminary Design Report
November 03	2010	Technical Design – Approval of Long Lead Term Procurement
January 11	2011	Start Lead Time Procurements (monochromators, CRL, enclosures,…)
April 14	2011	Complete Final Design of Beamline Major Components
February 07	2012	Complete Final Design Report Approval of Start of Beamline Construction - Beneficial Occupancy of Experimental Floor
February 10	2012	Start Installation
May 15	2012	Start Sub-System Testing
April 20	2012	Start Other Procurement
November 05	2012	Complete Long Lead Time Procurements
August 14	2013	End Procurement
August 19	2013	Start Integrated Testing
January 07	2014	Complete Installation
February 03	2014	Complete Sub-System Testing
May 27	2014	Complete Integrated Testing – Beamline available for Commissioning
June	2015	**CD-4**, Approve Start of Operations

APPENDIX 2 REFERENCE DRAWINGS

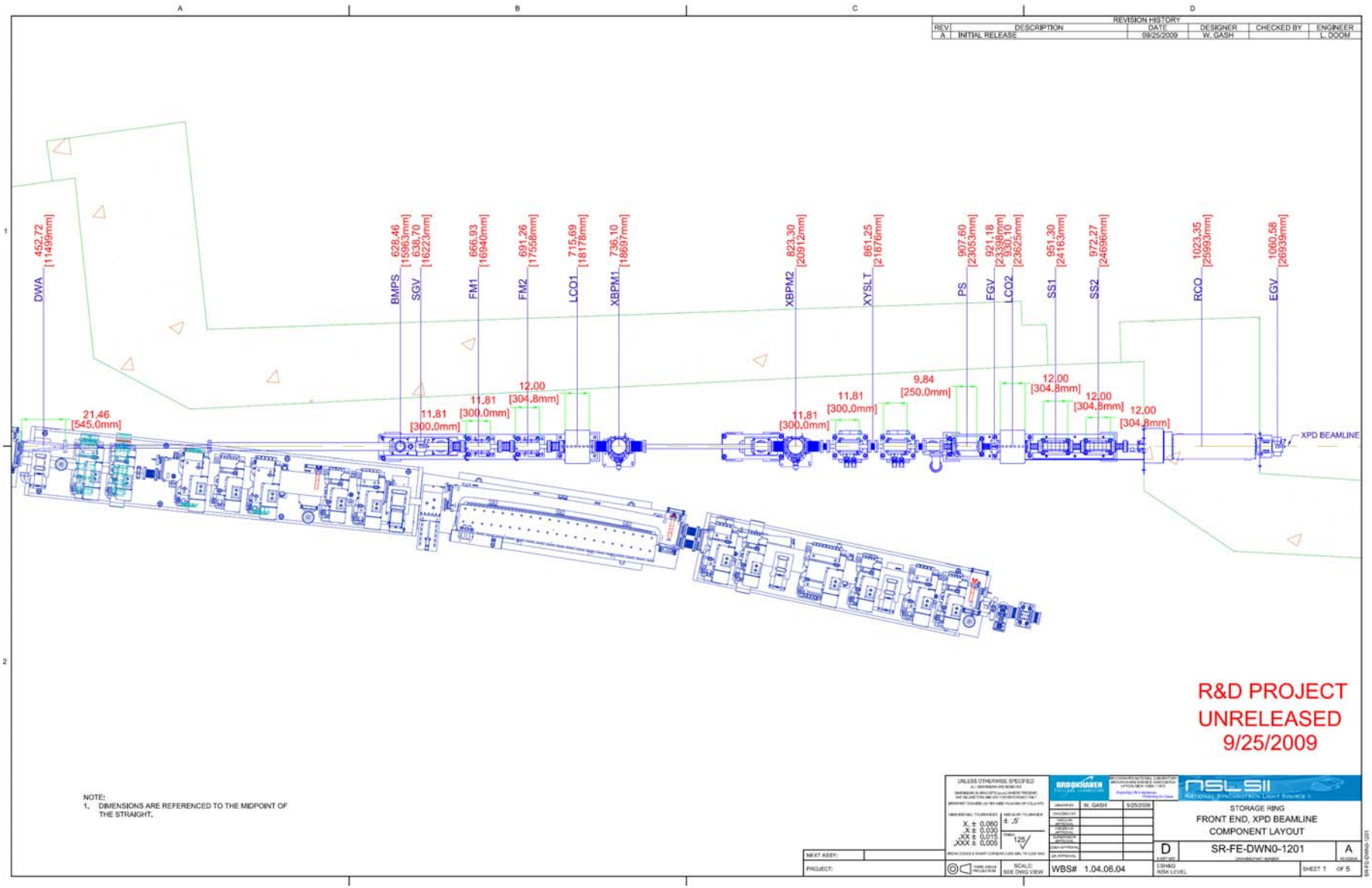

Front-end layout plan of the Front End of XPD (L. Doom).

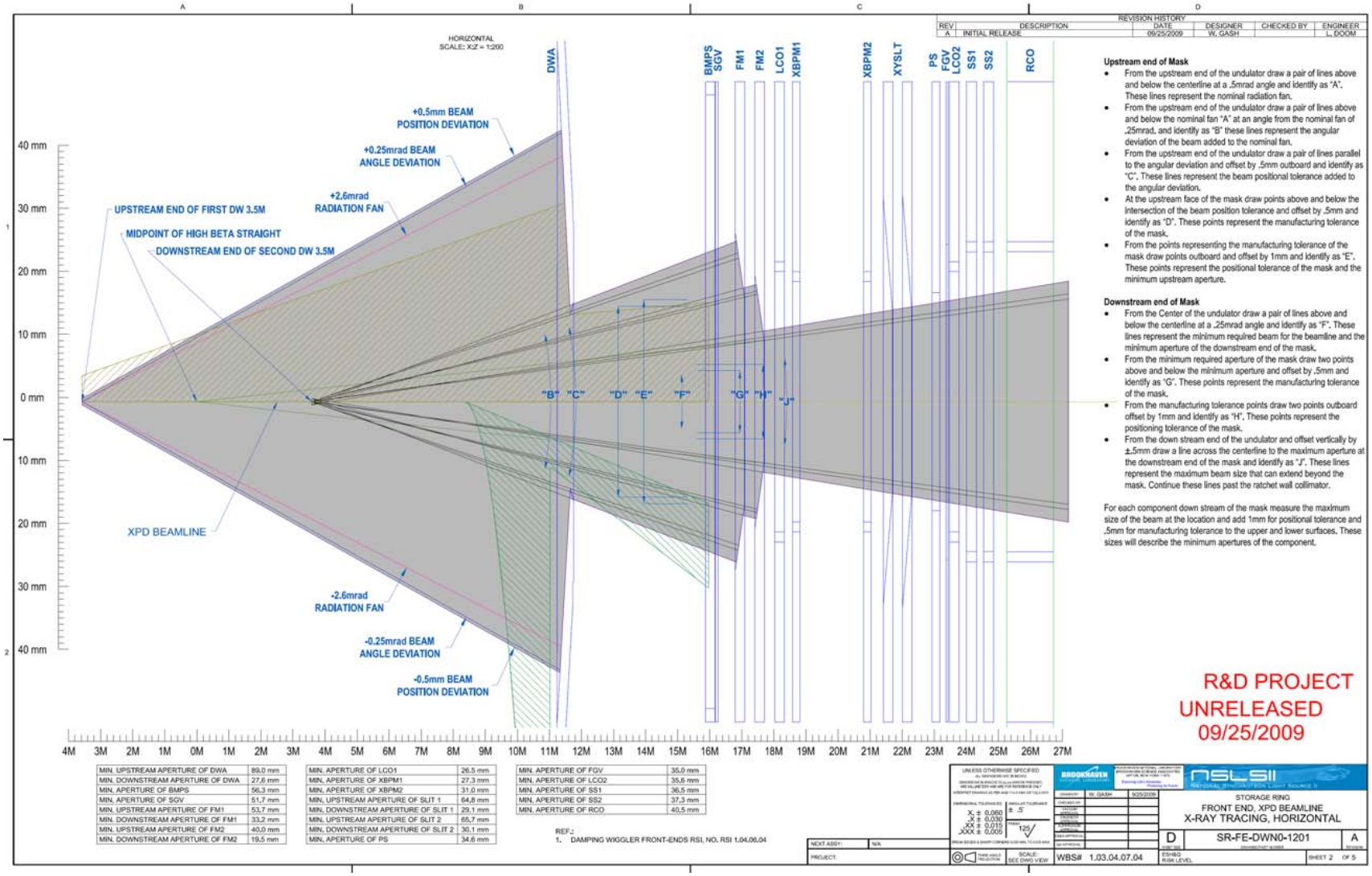

Preliminary Front End x-ray tracings (L. Doom).

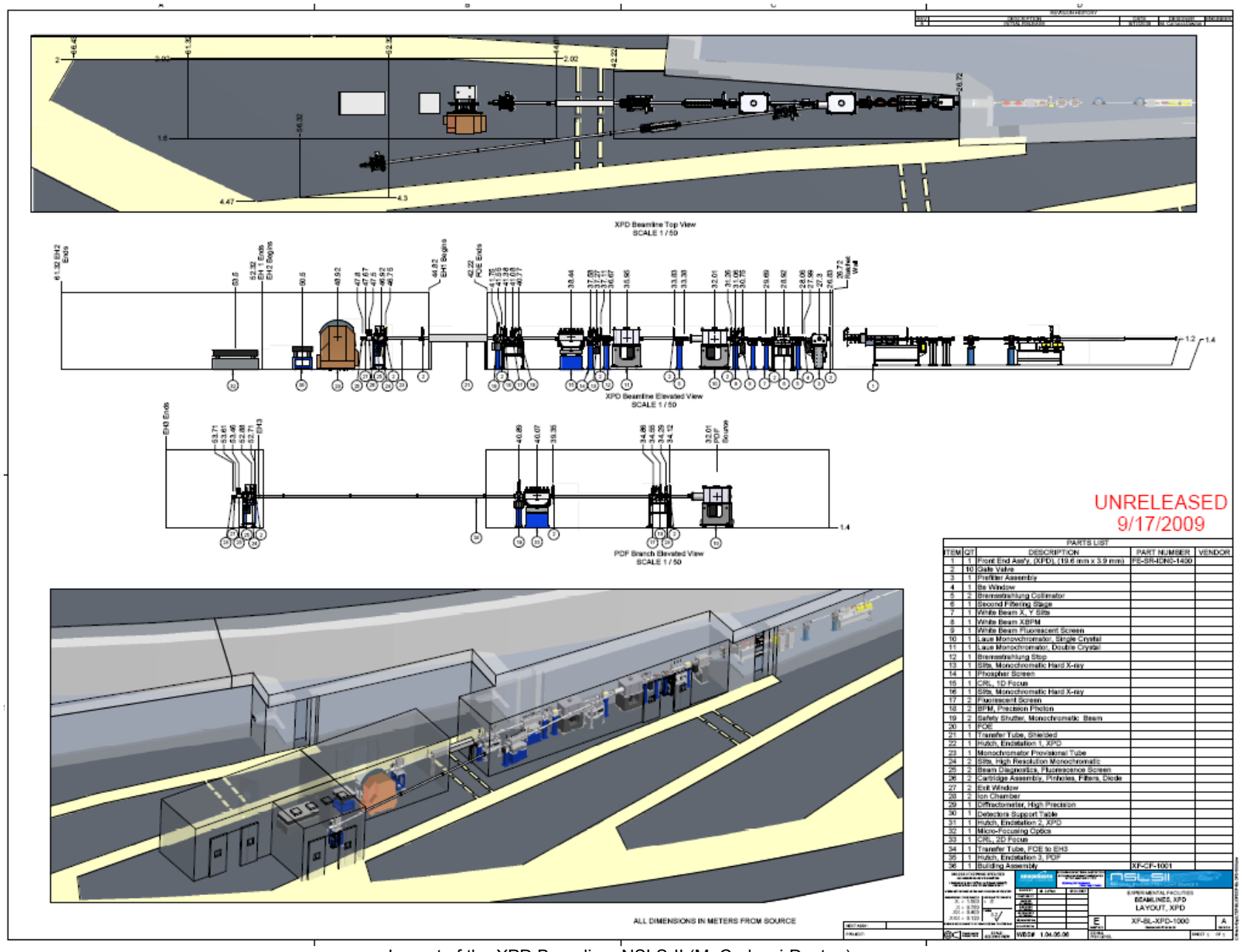

Layout of the XPD Beamline, NSLS-II (M. Carlucci-Dayton).

APPENDIX 3 REPRESENTATIVE EXPERIMENTS

In general, data are required that have the highest possible resolution both in reciprocal space and in real-space. These examples, as well as many more, are described in detail, with references, in the Materials Community White Paper and are provided here by way of example. The XPD Beamline will allow similar studies to be carried out, but under more challenging conditions, moving towards the ability to study these effects *in-operando* in devices that are heterogeneous on the sub-micron scale and where the species of interest are dilute and evolving in time.

a. Encapsulated materials: hydrogen storage

Pivotal to the rational development of host materials with increased H_2 storage capacities (approaching projected DOE targets for practical applications) is the understanding of the nature of the H_2 -framework interaction and the factors that influence H_2 binding strength and storage capacity. However, few structural studies have directly probed the adsorption sites in these systems when loaded with H_2. As such, the principal mechanism for H_2 sorption remains controversial and speculative, with the current views developed from attempts to correlate observed sorption behavior with the structural features and chemical functionality of the apo-host (e.g., surface area and volume; surface polarizability and potential coordination sites). In a recent PDF structural study of local H_2-framework interactions within the H_2/D_2 loaded Prussian Blue analogue, $Mn_3[Co(CN)_6]_2$, both high energy X-ray and neutron scattering data were used together. The results contradicted accepted models by demonstrating there is no evidence for binding interactions with the accessible MnII sites.

b. CO_2 sequestration: in-situ HP powder diffraction

Injection of Carbon (CO_2) as a means of oil recovery is a mature technology and is also seriously considered as a means of effective carbon sequestration. Despite a number of modelling studies there are relatively few experimental studies to examine the chemical processes that may occur down-hole when supercritical CO_2 is injected. One study showed dramatic changes in the solution chemistry raising questions about the long-term stability of injected CO_2 due to changes in the chemical environment. This environment may vary considerably with different minerals, brine concentration, pH, T, P. This has been the subject of an *in operando* study to examining the effects of these variable on the super-critical CO_2-rock interaction by the group of Pam Whitfield. Initial studies in the laboratory using a modified cell, that might serve as a prototype for NSLS and NSLS-II, show high pressure carbonation of wet wollastonite under relatively mild conditions (45-73ºC), followed by quantitative analysis of the data using Rietveld refinement, are consistent with results of thermal analysis results and more time consuming techniques.

c. Accelerated Design of Advanced Structural Ceramics

Once new materials have been identified and the volume and unit cell shape changes as well as transformation temperatures have been identified, structural ceramic composites can be designed and fabricated for *in situ* studies of stress-induced transformation toughening. Specifically, knowing the thermal expansion coefficients of candidate matrices and toughening phases, chemically compatible composites having matched thermal expansion coefficients can be engineered as laminates or fibrous monoliths, or even as fiber-reinforced composites. Bulk samples of such composites can then be prenotched and evaluated by *in situ* straining stage experiments under high energy x-ray radiation. The mechanisms of stress-induced transformation and the resultant redistribution of stress states, clamping forces of a propagating crack tip and overall toughening of the ceramic component can then be demonstrated. A specific example to illustrate such a composite would be transformation weakening of enstatite ($MgO{\bullet}SiO_2$) as a potentially debonding interphase in forsterite ($2MgO{\bullet}SiO_2$). High energy x-rays and small, well defined beams are required for these studies along with the ability to place and manipulate tensile stress equipment in the beam. Such information gives immediate feedback on the mechanism of strain toughening in ceramics that will accelerate the design of new materials.

d. Catalysts and catalysis

Many (if not most) catalysts have different structures while operating than they do at ambient conditions. Attempts to develop structure/activity correlations using only ambient structural information are thus doomed to failure. Development of improved catalysts requires in situ studies of real poly/nanocrystalline materials under operating conditions. Catalytic phases often contain many multiply- and partially-occupied sites, making determination of even their average structures a challenge. Catalytic properties often depend on the surface (not bulk) structure and/or the boundary regions between phases. The ability to point a very small x-ray beam on a desired region in a polycrystalline catalyst sample while operating will be crucial to making progress in understanding industrially-relevant systems. Compared to earth science systems, the temperature and pressure requirements for catalyst studies are modest, but systems for handling potentially-hazardous atmospheres need to be designed into the beamline.

APPENDIX 4 THERMAL CALCULATIONS

A more selective aperturing (central part of the fan), restricting the aperture to ~1mrad (H) × 0.1mrad (V), still leaves almost 6kW. Extreme filtering is being considered, using a multi-filter stage: C (5mm) and Si (8mm) filtering. The figure below shows that the power through a 1x0.1mrad^2 mask is progressively scaled down from 5.7kW to 2.3kW past the 5mm C pre-filter and 0.3kW after the 8mm Si filter stage. The residual incident power is 280W, of which 21W is absorbed in a 0.5mm Si crystal. This filtering strategy reduces the flux by 64% at 50 keV and 46% at 80keV.

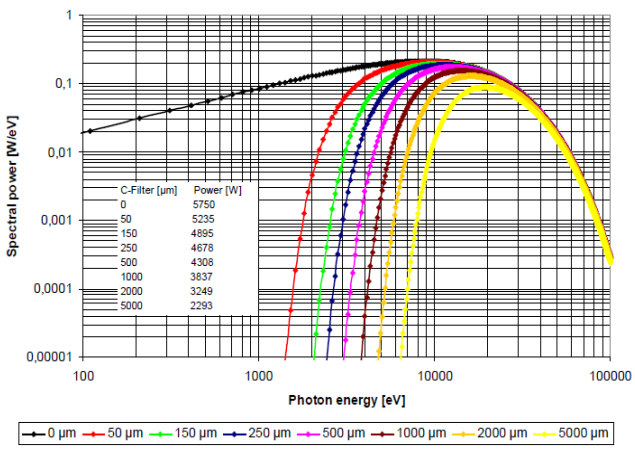

Carbon pre-filter transmission assuming a 1×0.1mrad^2 angular acceptance.

Carbon Pre-Filter Absorption for a 1 mrad by 0.1 mrad beam at 30 m.

Total filter thickness [µm]	Total power after filter [W]	Power density after filter [W/mm²]
0	5750	67.6
50	5235	61.9
150	4896	58.1
250	4678	55.6
500	4308	51.4
1000	3837	46.0
2000	3249	39.2
5000	2293	28.0

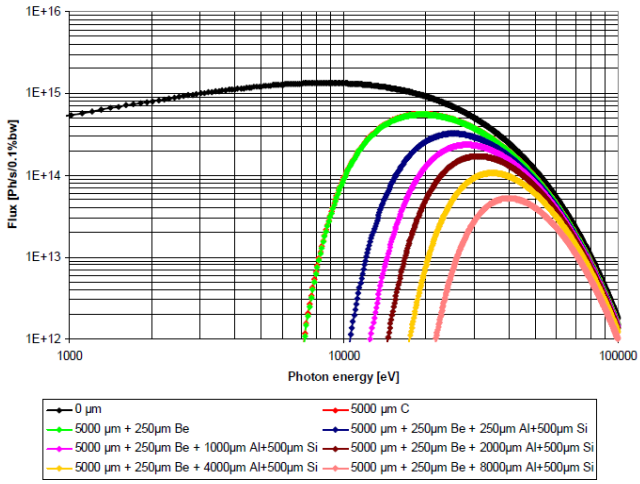

Effect of the second filtering stage on the spectral transmission assuming a 1x0.1mrad^2 angular acceptance.

Preliminary calculations were carried out by V. Ravindranath, assuming the monochromator is located at 25m from the DW source, the aperture size is 1mrad × 0.1mrad, the beam incidence angle = 45°, and the power absorbed by the crystal = 25W. Both sides of the crystal are at 25 °C (water cooling, see figure below). The peak temperature is found to be as high as 169°C. Assuming cryo-cooling (both sides of the crystal at -196°C), the peak temperature is -182°C and the resulting displacement (25nm) and the slope error (2.5µrad) are negligible.

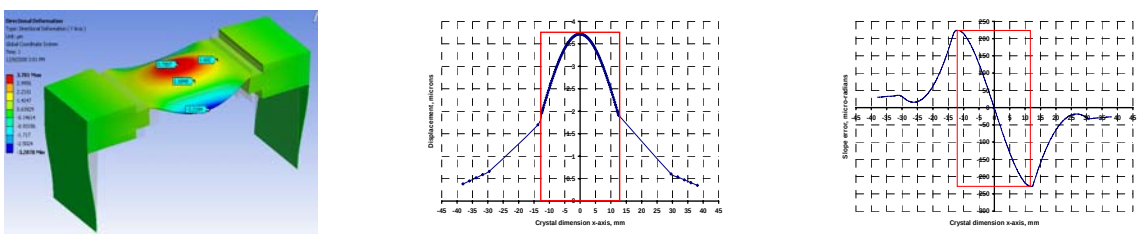

Water-cooled crystal: peak temperature = 170°C, displacement ≈3.8µm, and slope error ≈225 µrad in the transverse direction.

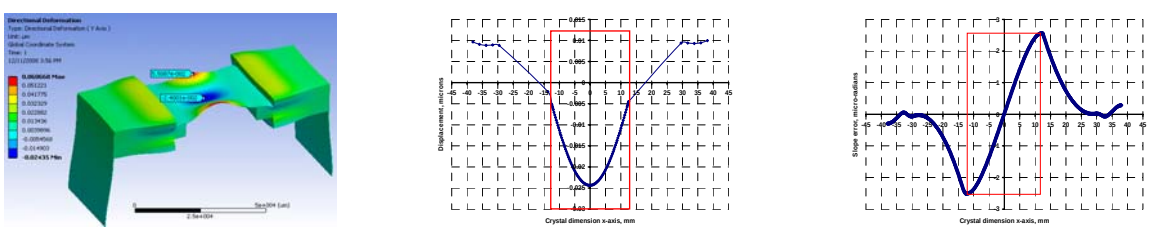

Cryo-cooled crystal: peak temperature = 91°K, displacement ≈25nm and slope error ≈2.5 µrad in the transverse direction

FEA calculations on the monochromator Silicon first crystal (V. Ravindranath).

APPENDIX 5 LAUE MONOCHROMATIZATION

Horizontal Deflecting Side Bounce Monochromator

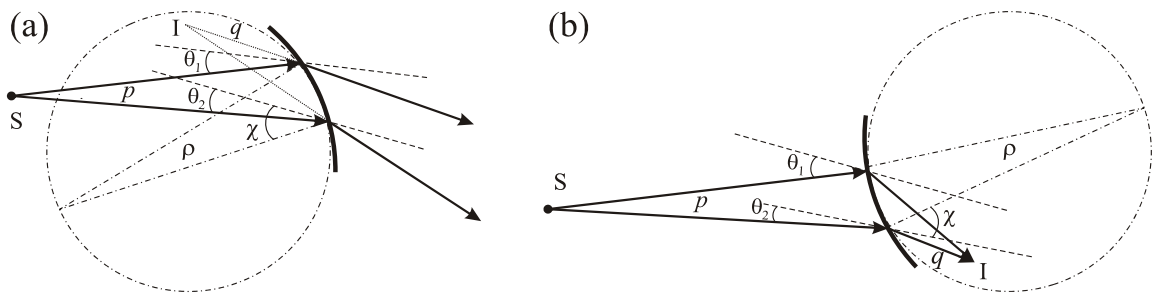

Top views of the horizontal focusing by cylindrically bent Laue crystals.

Two cases of the point-to-point polychromatic focusing by the cylindrically bent Laue crystals are shown: (a) if the incident beam is on the concave side of the crystal, the reflected beam remains diverging, while (b) a real image is obtained if the source is on the convex side. The relation between the bending radius (ρ), the source-to-crystal distance (p = 32m) and the crystal-to-image distance (q) is the following [16,17]:

$$p_o / p + q_o / q = 2 / \rho,$$

where p_o and q_o are those for monochromatic focusing (the source S and the image I are both on the Rowland circle), given by

$$p_o = \rho \cos(\chi \pm \theta_B),$$

$$q_o = \rho \cos(\chi \mp \theta_B).$$

Here θ_B is the Bragg angle and χ is the asymmetric angle between the Bragg planes and the surface normal of the crystal. We should note that these relations are derived for polychromatic focusing, which are the same as in the monochromatic focusing case only in particular cases: the symmetrical reflection or when the Rowland condition is achieved.

The energy bandwidth $\Delta E/E$ of the diffracted X-ray by a bent Laue crystal is given by [4]

$$\Delta E/E = \cot \theta_B \, [\Delta\theta^2 + \omega_0^2 + (\sigma_h/p)^2]^{1/2}$$

where $\Delta\theta$ is the variation of the incident angle due to the horizontal divergence ψ_h of the beam, ω_0 is the intrinsic angular acceptance of the crystal, and σ_h/p is the angular aperture of the horizontal source size. For the Damping Wiggler source at NSLSII, the desired horizontal beam size is small ($\sigma_h \approx 137\mu$m), which will introduce a $\Delta E/E$ less than 10^{-4}. For a flat perfect crystal, ω_0 is simply the Darwin width. For a bent crystal, ω_0 also accounts for the change in the Bragg angle across the crystal thickness (crystal distortion). When the bent is mild (close to the Rowland condition), ω_0 is less than 0.1mrad ($\Delta E/E < 10^{-3}$). Therefore, the energy bandwidth is mainly determined by the divergence term, which, for $\psi_h = h/p$, is given by

$$\Delta\theta = h \, [1/p_o - 1/p].$$

Following these equations, we must optimize (1) the energy bandwidth, (2) the beam spot size and (3) the reflectivity through the combination of the correct reflection plane, the bending radius (ρ), the asymmetry angle (χ) and the thickness of the crystal.

Two possible modes are suggested here: (a) the source is located on the concave side of the crystal. The energy bandwidth is easily reduced by bending the crystal close to the Rowland condition. However, with the 1mrad

horizontal divergence, the beam size will be about several centimeters without applying any slit. (b) The source is on the convex side of the crystal. The beam will converge to a pseudo-focus. However, the energy bandwidth will be too large ($>10^{-2}$). A pre-crystal aperture ($\leq$ 0.2mrad) will be needed in order to reduce $\Delta E/E$ to 5×10^{-3}. As a result, the total flux will be also reduced by 80%. An alternative way will be using another bent crystal after the side bounce as a secondary monochromator. The following discussion will focus on the mode (b).

Since the side bounce angle ($2\theta_B \approx 7^o$) is preselected, four possible optimized energies are calculated using different reflection planes. The ray tracing and calculation were performed using the SHADOW VUI 1.0. The Damping Wiggler source simulated in SHADOW indicates a photon beam size (FWHM) of 0.34mm (h) × 0.013mm (v), and the angular divergence (FWHM) of 2.5mrad (h) × 0.1mrad (v) at the waist for the photon energies above 50 keV. (These spatial properties need to be further verified). In these calculations, the full vertical fan was accepted, and therefore, remained the near-Gaussian profile. By applying the fixed mask aperture, the horizontal aperture was chose to be 0.2 mrad in order to reduce $\Delta E/E$. Contrastable results obtained with 1.0mrad aperture are also listed in the table below (numbers in the parentheses). The horizontal beam size at the crystal is 7.0 mm for 0.2mrad aperture and 35mm for 1mrad aperture. The bending radius ρ was optimized to achieve the smallest horizontal spot size at 8m after the crystal (where the CRL is located). The fluxes per millimeter over the horizontal plane at 8m after the crystal were then calculated using

$$I = I_o\, N_r \Delta E/N_i/E/\delta_h$$

where I_0 is the incident flux, N_i is the number of the incoming rays, N_r is the number of the reflected rays recorded by SHADOW, ΔE is the photon energy bandwidth over which the ray tracing was performed, E is the central photon energy and δ_h is the horizontal spot size at 8m after the crystal. The source fluxes I_0 (ph/s/0.1%BW/mrad) are given in the table.

Side bounce Laue monochromator calculation corresponding to: p = 32m, q = 8m (CRL location), pre-crystal horizontal aperture = 0.2mrad (and 1mrad shown in the parentheses), σ_h = 137μm, crystal thickness T_0 = 0.5mm (X. Shi).

(Reflection)<Crystal cut>	(311) <511>	(331) <100>	(422) <100>	(511) <111>
χ: (°)	60.5	43.5	54.7	51.1
E: (keV)	60	80	90	95
I_0 at E: (ph/s/0.1%BW/mrad)	8.8×10^{13}	1.7×10^{13}	7.2×10^{12}	4.7×10^{12}
$2\theta_B$: (°)	7.24	7.13	7.12	7.16
ρ: (m)	60	35	50	45
$\Delta E/E$: (10^{-3})	4.7 (≈30)	4.5 (≈30)	4.4 (≈30)	5.1 (≈30)
δ_h at 8m after the crystal: (mm)	1.3 (3.8)	1.0 (3.3)	0.96 (3.1)	0.93 (3.1)
I: (ph/s per horizontal mm)	5.1×10^{11} (6.3×10^{11})	7.1×10^{10} (6.7×10^{10})	2.0×10^{10} (1.2×10^{10})	6.0×10^{9} (4.5×10^{9})

In the horizontal plane, for the 0.2mrad aperture, the beam size can be focused by the crystal from 7mm to 1mm, which is similar to the ratio observed at NSLS X17A (from 3mm to 0.5mm). However, the CRL is still needed for further focusing to the sample. In the vertical plane, if we apply the sagittal curvature to the crystal, we can focus the beam to the sample directly.

Sagittally-Focusing Double-Crystal Laue Monochromator

If a point divergent source is used, the distance from the source to the crystal F_1 and the distance from the crystal to the focal point F_2 are then related by:

$$1/F_1 + 1/F_2 = 4 \sin\theta_B \sin\chi / R_s,$$

while ignoring the distance in between the two crystals. In order to increase the energy resolution, both crystals should fulfill the Rowland condition. While R_{m1} can be calculated through eq. (3), R_{m2} is related to R_{m1} through

$$R_{m2}/R_{m1} = \cos(\chi_1 - \theta_B)/\cos(\chi_1 + \theta_B).$$

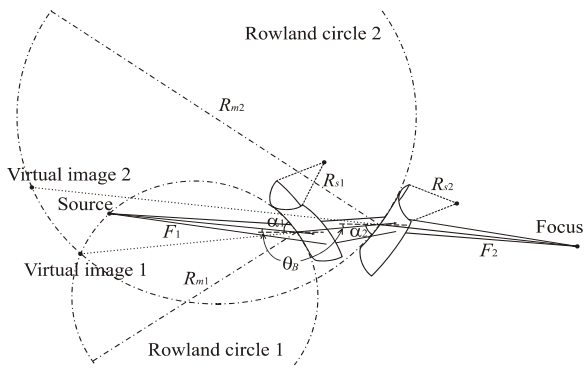

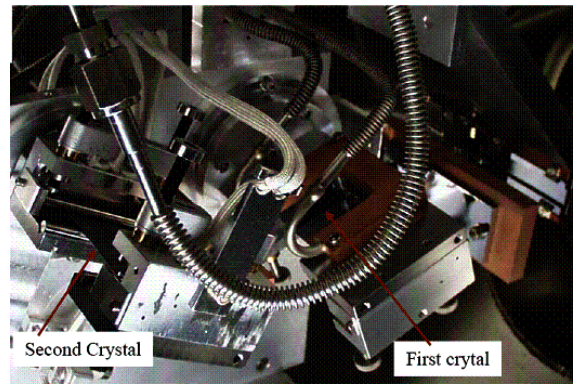

(left) Geometry of a sagittal bent double-Laue monochromator;
(right) Monochromator installed at the NSLS X17B1 beamline.

The bent Laue system provides over an order of magnitude more flux with a reasonably low increase in energy spread. This more than tenfold flux enhancement results from the bending strain-induced broadening of the crystal reflection angular acceptance. The anticlastic bending facilitates the use of the inverse-Cauchois geometry in the meridional plane to provide better energy-resolution and to increase the photon flux. The anticlastic bend radius needs to be properly adjusted so that all rays make the same incidence angle with respect to the crystal planes (the so-called Rowland condition). This new x-ray optics concept makes it possible to focus the large divergence of high-energy x-rays produced by the NSLS-II damping wiggler. For many experiments, with a vertical scattering plane geometry, beam divergence of the order of 0.1-0.2mrad at the sample and the modest 10^{-3} energy spread will be tolerable. A larger divergence (1mrad) in the horizontal plane also is acceptable.

A double-crystal sagittally focusing monochromator has been constructed and tested, and has been in use at the X17B1 beamline for the past two years, providing 67 keV x-rays (figure above). It focuses a horizontal divergence of 3mrad to a brightness-limited horizontal dimension of 0.2mm. The x-ray flux-density at the focus was a few hundred times larger than that of unfocused x rays. A similar design has also been implemented at X7B: our recent tests at X7B show the horizontally focused beam image at E=38.925keV, showing a demagnification factor of ~30.

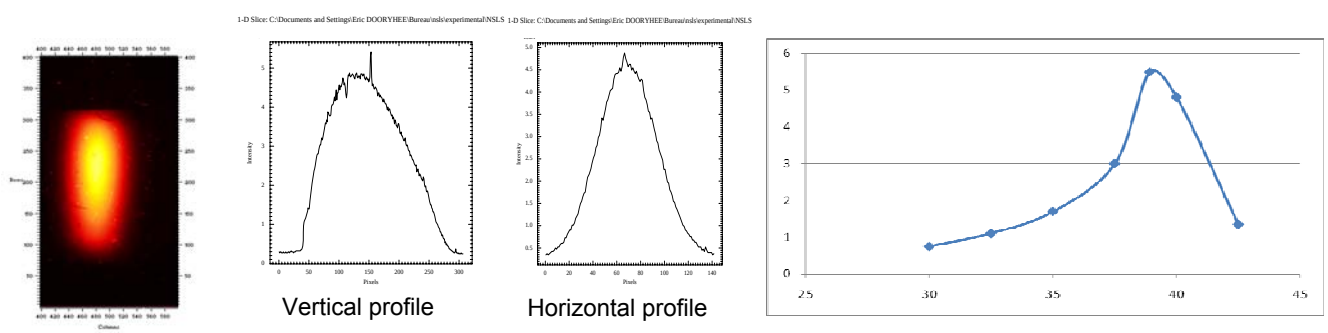

The beam size at the monochromator approximately is 25mm (2mrad horizontal fan) by 2mm (V). The source-to-monochromator distance is 11.026m. The monochromator-to-sample distance is 12.344m. The final optimized focused image at E=38.925keV is shown above: horizontal FWHM ~0.75mm, vertical FWHM ~2mm. With no bending readjustment, the maximum intensity amplitude of these profiles varies by a factor of 7 over the 30 to 42.5keV energy range.

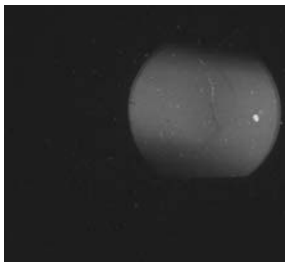

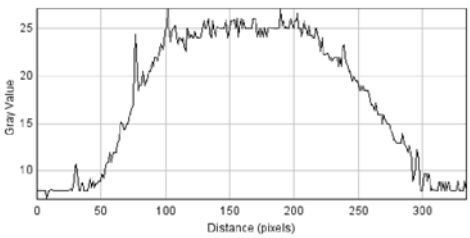

Horizontal Profile at 30keV

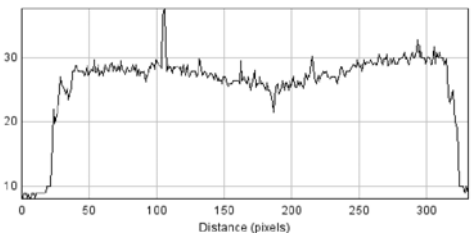

Vertical Profile at 30keV

Out-of-focus image of the beam (collimator truncated) and the corresponding horizontal and vertical profiles at 30keV, keeping the crystal bend setting unchanged between 38.9keV and 30keV.

APPENDIX 6 REFRACTIVE OPTICS

Although the CRL are more suitable for small divergent (undulator) beams, they can match the wiggler beam divergence (up to 100μrad) if they are close enough to the source. We can have them placed before the monochromator for two main reasons:

- The vertical and horizontal beam size has to be tailored to the acceptance of the lenses which typically is 1-2 mm. At a distance of 30 m from the source, the vertical beam size already would be about 3-4 mm. Therefore, moving the CRL closer to the source thus captures a larger proportion of the diverging x-rays. The situation gets far worse in the horizontal direction, *making the development of 1D focusing optics a major request for XPD*.
- Collimating the beam in the vertical beam yields a vertical divergence which better matches the angle acceptance of a high-resolution monochromator first crystal (typically 10μrad at 50keV), improving the performance and flux output of the monochromator.

However, the Laue-Laue monochromator uses the Rowland geometry whereby the anticlastic meridional curvature of the crystals matches the vertical divergence. There is no need for collimating the beam before the monochromator. Therefore, the 1D CRL will be placed after the monochromator (source-to-CRL distance = 38.4m in the main line). *This option relies on the on-going developments regarding 1D focusing and larger acceptance CRL*.

The situation is different in the branchline, for the CRL are placed close to the secondary source produced by the single-bounce monochromator.

In the design of the refractive lenses, we are considering 4 different profiles:

- Parabolic [18]
- Triangular/parabolic saw tooth [9]
- Kinoform profile [19,20]
- Prism [21]

The current proposal would allow for different sets of lenses. The long set will be used to focus (converge) photons with energies larger than 80 keV. The short set will be used to focus (converge) at around 50keV and also can be used to partially collimate the high-energy photons above 80keV. Below we present examples of lenses configurations.

At 80keV main branch	
Number of lenses	~110
Demagnification (p/q)	2.7
Acceptance (mm)	~1
Length (mm)	~150
At 50keV	
Number of lenses	~40
Demagnification (p/q)	2.7
Acceptance (mm)	~1
Length (mm)	~120

The exact parameters of the CRL assembly should be calculated after a final decision on the focal spot sizes and depending on the final position of the lenses and DLCM [9].

APPENDIX 7 DETECTOR DEVELOPMENT

1D and 2D area detectors are increasingly used for powder diffraction. They can considerably improve the detection of very weak signals, and help improve the detection limit to identify intermediate steps in the synthesis or processing of a material. Time resolution takes precedence over angular resolution, requiring a high efficiency photon counting 1-2D detector with sub-sec time resolution. Fast acquisition rate is also required for applications such as diffraction imaging [22] or diffraction tomography [14]. Energy discrimination also is useful in those high-energy measurements where the inelastic (Compton) background could be screened out electronically, and the signal-to-background ratio improved. Higher quality of data can be achieved in the high-Q range.

A good scattering sample only requires a detector image plate, such as the MAR555 (140μm × 140μm pixel size, 430 × 350mm^2, ~1 Hz, 18 bit contrast resolution), be exposed for a few hundred microseconds. Yet the readout of this image (including erase cycle and control macro completion) requires approximately 90s. The MAR345 image plate scanner (circular active area of diameter 345 mm with a pixel size of 150μm or 100μm depending on the readout mode) is also a widespread high-energy detector, but the Point Spread Function deteriorates the pixel size by ~3 and the efficiency at 90keV is as low as 10%.

Faster area detector options are available, including coupling of image intensifiers, or scintillation screens with taper optics, to fast fiber-tapered CCD cameras. However, generally speaking, many of these systems suffer from variable image distortions, low resolution and/or small detection areas.

Mythen strip array detectors (PSI design) are being used at the DIAMOND, SLS and Australian synchrotron facilities and our design will incorporate similar technology; a 7000-element silicon strip detector array (0.014° angle and ~350eV energy resolution, ~1ms readout time) is currently being fabricated at NSLS for in-situ real time material studies. The specifications of the NSLS 1D Si-array are:

- 4mm × 0.125mm strips in arrays of 384 and 640 strips
- Fully-depleted 0.4mm thick detectors
- Pitch matched to ASIC, so simple bonding to form arrays
- 350eV energy resolution @ 5.9keV
- 10^5 cps per strip maximum counting rate
- Readout of 640 strips in few ms.
- Peltier and water cooling

The CMOS-based digital flat-panel detector technology represents a significant step forward for high-energy x-ray diffraction [23-25]. The Pixium 4700 detector [25] combines an amorphous Si panel with a Tl-doped CsI scintillator layer. The detector has a useful pixel array of 1910x2480 pixels with a pixel size of 154 microns, and thus it covers an effective area of 294mm × 379mm. Designed for medical imaging, the detector has good efficiency at high x-ray energies. Furthermore, it is capable of acquiring sequences of images at 7.5 frames per second in full image mode, and up to 60 frames per second in binned region of interest modes. The detector exhibits a narrow point-spread function and a distortion-free image, most appropriate for the acquisition of high-quality diffraction data. In addition, high frame rates and shutterless operation open new experimental possibilities. The sensitivity of the a-Si detector to high-energy X-rays is enhanced, in addition to the increase in experimental efficiency accompanying the virtually continuous exposure/readout.

The General Electric Healthcare detector has similar features [23,24]). Perkin-Elmer also offers a similar design, whose characteristics are 200μm × 200μm pixel size, 410mm × 410mm field of view, 15Hz readout, 16-bit contrast resolution. The scintillator is made of CsI, and proves to perform well at 90keV.

Another relevant development is the photon-counting pixel detector, such as XAMPS (developed at NSLS) or XPAD (CNRS, France [26,27]), MediPIx [28] or PILATUS II (PSI-SLS [29]). A pixelated detector offering a spectrum-per-pixel response, with adequate energy and spatial resolution, opens the breach to simultaneous spectroscopy/diffraction experiments. As an example, the parallel architecture of the XPAD detector design allows

to collect 423 images with less than 10ms exposure (16 bits) or 233 images exposed for more than 10ms (dynamic range=32 bits). In both cases the deadtime between two consecutive images is no more than 2ms; it will be further reduced below 1µsec with buffered output logics in next generation detectors [27]. The full diffraction "movie" is transferred afterwards to the acquisition station after the measurement via a 100MB ethernet link. Some applications of a hybrid pixel detector to powder diffraction is given in reference [30]. Typical pixel size can be 130µm and continues decreasing. For XPAD, the saturation rate is 10^5 photons/s/pixel and the noise level is < 0.1 photon/s/pixel. Replacement of 500µm Si by 700µm CdTe is currently being tested.

The scientific case emphasizes the need for time-resolved/fast studies, and 1kHz acquisition rate is anticipated to become routine work in the future. Recently, Labiche et al. [31] studied the change of iron oxidation:

$$4Fe_2O_3 + 4Fe + NaClO_4 \rightarrow 4Fe_3O_4 + NaCl$$

as a test case, using the FReLoN2k camera: 8,192 diffraction patterns using 64x2048 ROI and 64x2 rebin were collected at a rate of 50Hz, i.e., 19ms integration time and 1ms for data processing and transfer.

The detection (~absorption) efficiency at 100keV of Si 0.5mm, Ge 0.5mm and Ge 1mm is 2%, 14% and 25%, respectively. This drastically limits the efficiency of Si-based detector technology, and the problem arises from the material itself. Thicker scintillators or sensors do not really help: parallax error, lateral spatial resolution degrades with layer thickness, high depletion voltage,… The higher mobility of carriers combined with low effective mass in Ge, as compared to Si, has generated a lot of interest in Ge-based devices. The challenge is having a robust barrier oxide since native Ge oxide is hygroscopic. Other alternatives on semiconductor sensors currently under investigation include: GaAs, CdTe or CdZnTe, n/p Ge, ZrO_2 and HfO_2 on Ge. High-Z scintillating screens from YAG:Ce to LAG:Eu are also being explored.

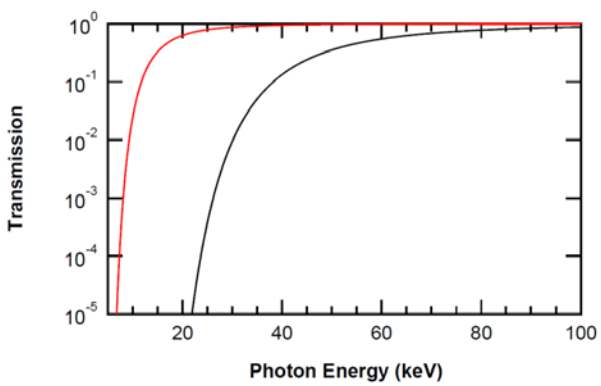

Transmission efficiency of 250µm Si and Ge as a function of x-ray energy.

The technology currently used for making germanium-based sensors is not amenable to making monolithic planar segmented devices such as microstrip detectors. The NSLS Detectors Group is aiming at developing this technology, and subsequently, detectors based on these sensors. *The design of an energy resolving wide-angle photon counting Ge strip detector* (~11 individual modules tiled to provide the necessary angular 100° coverage, 250µradian resolution on 0.5m radius, cryogenic cooling) with good efficiency at around 75keV, would have a tremendous impact on the beamline performance.

For crystallography challenging materials, an important breakthrough can be made with improved detector technology over the high-energy x-ray range. Expected figures in the next 5 years are :

- Time slicing ≤ 1ms or frame rate ≥ 1 kHz (kinetics)
- Pixel size ≈ 100µm × 100µm, i.e. angle resolution ~0.02° 2θ at 0.3m compared to 0.001° 2θ for a point detector with analyzer.
- Active area ≥ letter or A4 format for reaching high Qmax

Using "active" detectors would also be a significant step forward: photon counting with a Poisson statistics for physical interpretation of the data, improved readout schemes (e.g. multiple frame accumulation during the same

data acquisition cycle, using more registers per individual pixel), adjustable gain (counting individual photon up to ~10^{10} photons/s over strong diffracted peaks), image saving only when a random event of interest occurs.

The management of improved detector technology also relies on:

- detector control and interface software
- Integration in data acquisition board and scripts
- data transfer link,
- hard disc writing speed
- size of the available memory
- Data archiving/retrieval and metadata
- On-line data analysis: data screening, assessment
- On-line conversion from detector images into scientific images

Intentionally blank.